March 12, 2025

Vasopressin-Dependent β-Catenin Phosphorylation at Ser552 and Branching Structure of Mouse Collecting Duct System

Shuo-Ming Ou, Hiroaki Kikuchi, Euijung Park, Chin-Rang Yang, Viswanathan Raghuram, Shaza Khan, Adrian Rafael Murillo-de-Ozores, Lihe Chen, Chung-Lin Chou and Mark A. Knepper

Epithelial Systems Biology Laboratory, Systems Biology Center, National Heart, Lung, and Blood Institute, National Institutes of Health, Bethesda, Maryland, USA.

Running title: β-catenin phosphorylation

Keywords: aquaporin-2, cortical collecting duct, vasopressin, protein kinase A

Correspondence: Mark A. Knepper, MD, PhD, Systems Biology Center, National Heart, Lung and Blood Institute, 10 Center Drive, National Institutes of Health, Bethesda, Maryland 20892-1603 Phone: 1.301.496.3064 E-mail: knepperm@nhlbi.nih.gov

Emails: shuo-ming.ou@nih.gov; hkikuchi.kid@tmd.ac.jp, euijung.park@nih.gov; yangc3@mail.nih.gov; viswanathan.raghuram@nih.gov; lihe.chen@nih.gov; shaza.khan@nih.gov; chouj@nhlbi.nih.gov; adrian.murillodeozores@nih.gov; okokyytt@gmail.com; hkikuchi.kid@tmd.ac.jp; ray.mejia@nih.gov; knep@helix.nih.gov

Key points

- **Vasopressin regulates collecting duct (CD) transport by triggering phosphorylation of multiple proteins including β-catenin at Ser552.**

- **Mutating Ser552 to a non-phosphorylable amino acid in mice resulted in altered CD branching without loss of differentiation in adult CDs.**

- **The findings point to a role for β-catenin Ser552 phosphorylation in CD branching and sub-segmental CD elongation.**

Abstract

Background. Phosphoproteomics studies in both cultured and native collecting duct (CD) cells showed that vasopressin strongly increases PKA-dependent phosphorylation of β-catenin at Ser552. Relatively little is known about the role of Ser552 phosphorylation.

Methods. To address the role of β-catenin Ser552 phosphorylation in the mature renal CD, we have inserted a Ser552Ala mutation in mice using CRISPR-Cas9.

Results. The mutation did not affect the renal abundance of the vasopressin-regulated water channel aquaporin-2 (AQP2) or urinary osmolality. However, the structure of the CD system was altered. Specifically, the cortical branching ratio (the number of nephrons that merge to form one cortical CD) was reduced from 6.18 ± 0.66 in control mice to 3.33 ± 0.82 in Ser552Ala mutant mice. This was associated with a greater number of cortical and medullary CDs with smaller average diameter. The total number of nephrons (glomerular counts) was not different between control and Ser552Ala mutant mice (both ~13,500 per kidney). RNA-seq in microdissected cortical CDs of the mice revealed a highly significant enrichment of genes involved in regulation of mitosis and the cell cycle, along with decreases in mRNAs coding for two CDK inhibitor proteins, *Cdkn1b* and *Cdkn1c*. At the same time, there were no changes in abundances of major transporter mRNAs, indicative of sustained CD differentiation. A subset of cortical CD cells showed an increase in DNA content, consistent with G2/M cell-cycle arrest.

Conclusions. The observed structural changes in the collecting duct system of adult mice point to a role of vasopressin-mediated post-translational modification of β-catenin at Ser552 in collecting duct development, presumably PKA-mediated Ser552 phosphorylation. We speculate that vasopressin may act to slow or halt branching morphogenesis perinatally and may affect the collecting duct elongation process that normally produces the unbranched region of the CD system in the cortex and outer medulla.

Introduction

Acting through the V2 receptor (V2R), vasopressin has a variety of structural and functional effects in renal collecting duct principal cells in the mature collecting duct including increased *Aqp2* gene transcription,[1, 2] increased aquaporin-2 (AQP2) protein half-life,[3, 4] increased principal cell size,[5-8] increased exocytosis of AQP2-containing vesicles,[9-11] decreased AQP2 endocytosis,[10, 12] increased active Na^+ reabsorption,[13, 14] reorganization of actin filaments,[15-19] and a decreased rate of apoptosis.[20] Signaling is via the $G_\alpha s$/adenylyl-cyclase/cyclic-AMP/protein-kinase-A(PKA) pathway.[21-23] Phosphoproteomic analysis of the effects of vasopressin has identified a number of target proteins that may be responsible for the structural and functional consequences of vasopressin signaling.[24] Among these targets is β-catenin (Gene symbol: *Ctnnb1*), which undergoes a marked increase in phosphorylation at serine-552 (Ser552) in response to vasopressin, based on both protein mass spectrometry and immunoblotting (**Figure 1**).[25-29] Here, we investigate the role of Ser552 phosphorylation of β-catenin in the structure of the collecting duct system, using CRISPR-Cas9 to mutate the site to a non-phosphorylatable amino acid.

Prior studies have implicated the Wnt pathway and β-catenin in the regulation of collecting duct branching during renal development.[30-32] It is well established that the collecting duct system is derived from the ureteric bud. The detailed morphometric study of Cebrián *et al*.[33] has tracked the changes in collecting duct architecture from the initial branching event around gestational age 11.5 to birth. Repeated dichotomous branching produces a relatively uniform pattern through gestational age 15.5 with approximately equal distances between branch points.[33] However, starting at gestational age 15.5, when the outer medulla begins to develop, elongation of the outer medullary portion of the collecting duct occurs to produce the long 'unbranched segment', originally observed by Karl Peter[34] and Jean Oliver[35]. The detailed and meticulous morphometric studies of Short *et al.*[36] in mice have demonstrated similar timing and have shown that branching development continues for a few days after birth. Our

own extensive studies involving microdissection of cortical collecting ducts (CCDs) from adult rabbits, rats and mice (see for example[37-39]) have shown that the unbranched portion of the collecting duct system extends from the outer medulla into the medullary rays of the cortex. The medullary rays are finger-like projections of the outer medulla into the cortex and are made up of a parallel arrangement of CCDs, cortical thick ascending limbs and S-2 proximal straight tubules. Thus, in the adult kidney, the long unbranched region consisting of the outer medullary collecting duct (OMCD) and the medullary ray portion of the CCD separates two branched regions, one in the cortical labyrinth the other in the inner medulla.

Collecting duct principal cells first become sensitive to vasopressin as they mature perinatally and presumably this is the time when vasopressin-induced phosphorylation of β-catenin at Ser552 first occurs.[40, 41] That is, vasopressin sensitivity of collecting duct cells coincides with the final stages of branching and formation of the long unbranched collecting duct in the outer medulla and cortical medullary rays. Given the known role of β-catenin in collecting duct development,[30-32] we hypothesized that mutation of Ser552 to an unphosphorylatable amino acid could alter the ultimate branching architecture of the adult mouse collecting duct system.

Methods

Mice. All animal experimental procedures were carried out in accordance with National Heart, Lung, and Blood Institute [NHLBI] animal protoco**l H-0047R6**, approved by the NHLBI Animal Care and Use Committee. Pathogen-free, male, 6-to 8-week-old C57BL/6 mice (Taconic) were used. In order to generate the Ctnnb1 T551A/S552A knock-in mutant mice, CHOPCHOP (https://chopchop.cbu.uib.no) was employed to obtain all the possible sgRNAs, and one sgRNA (CAACGGCGCACCTCCATGGG) was selected and purchased. A single-strand donor oligonucleotide containing the desired mutation was synthesized (IDT, https://www.idtdna.com/pages). The sgRNA (5 ng/ul) and donor oligonucleotides (100ng/ul) were co-microinjected with Cas9 mRNA (20 ng/ul) into the pronuclei of zygotes collected from C57BL/6 mice. Donor nucleotide sequences are given in Supplemental Figure 1 (https://esbl.nhlbi.nih.gov/Databases/Catenin-RNA-seq/Data/). Injected embryos were cultured in M16 medium overnight in a 37 ^{o}C incubator with 6% CO_2. In the next morning, embryos at 2-cell stage of development were implanted into the oviducts of pseudo-pregnant surrogate mothers. Offspring born to foster mothers were genotyped by PCR and Sanger Sequencing.

Urinary osmolality. Spot urines were collected by holding the mice over a piece of parafilm. Osmolality was determined by vapor pressure osmometry (Wescor).

Cell culture. mpkCCD cells, a mouse collecting duct cell line, were cultured and then seeded on semipermeable Transwell (Corning #3450) membranes. The cells were grown in complete medium (DMEM/Ham's F12 Gibco medium with 5 µg/ml insulin, 50 nM dexamethasone, 1 nM triiodothyronine, 10 ng/ml epidermal growth factor, 60 nM selenium, 5 µg/ml transferrin, and 2% fetal bovine serum). And then, the medium was changed to serum-free simple medium (DMEM/Ham's F12 Gibco medium containing only 50 nM dexamethasone, 60 nM sodium selenite, and 5 µg/mL transferrin) for 3 days to induce mpkCCD cell differentiation and complete polarization. Cells were exposed to dDAVP (0.1 nM) or

vehicle for various time periods. We also used mpkCCD cells in which both protein kinase A (PKA) catalytic genes (*Prkaca* and *Prkacb*) were deleted.[42]

Immunoblotting. Immunoblotting was carried out in either kidney tissue or cultured mpkCCD cells using procedures standard in our laboratory.[43, 44] Antibodies are identified in figure legends.

Microdissection of CCDs and branched connecting tubule (CNT)/ initial collecting tubule (iCT) structures. Mice were euthanized via cervical dislocation. The kidneys were perfused via the left ventricle with ice-cold Dulbecco's PBS (DPBS; Thermo Scientific), followed by reperfusion with the dissection buffer (5 mM HEPES, 120 mM NaCl, 5 mM KCl, 2 mM $CaCl_2$, 2.5 mM disodium phosphate, 1.2 mM magnesium sulfate, 5.5 mM glucose, 5 mM Na acetate, pH 7.4) with 1.5 mg/ml collagenase B (Roche). The collagenase-perfused kidneys were harvested and cut into thin slices along the cortical-medullary axis with a sharp razor blade. The digestion was continued in vitro in the same collagenase-containing dissection buffer. The digestion was monitored until optimal for single tubule microdissection, typically ~30 minutes. The microdissection of CCDs or branched CNT/iCT structures were carried out under a Wild M8 dissection stereomicroscope equipped with on-stage cooling. The collecting ducts were washed by transferring them to dishes containing ice-cold DPBS and manually 'swimming' them into debris-free fluid using a pipet or sharpened tungsten needle.

Immunocytochemistry of microdissected CCDs or branched CNT/iCT structures. After the branched CNT/iCT structures or CCDs were isolated, tubules were transferred to a glass bottom culture dish (MatTek, #P35G-0-20-C) coated with Cell-Tak (Corning, # CLS354241-1EA). The tubules were then fixed for 20 minutes with 4% paraformaldehyde in PBS and permeabilized for 20 minutes with permeabilization buffer (PBS with 0.3% Triton X-100 and 0.1% BSA). After permeabilization, tubules were blocked for 30 minutes with blocking buffer (PBS with 1% BSA and 0.2% gelatin). Primary and secondary antibodies are indicated in the figure legends. The anti-Na^+/K^+ ATPase antibody was produced in our laboratory by immunizing rabbits or chickens with a synthetic peptide corresponding to

the entire COOH-terminal tail of mouse ATP1A1 protein (sequence C-DEVRKLIIRRRPGGWVEKETYY) conjugated to keyhole limpet hemocyanin (KLH).[45]

Morphometry of microdissected CCDs. Determination of the numbers of cells per unit length in microdissected CCDs from the mice was carried out using DAPI to label nuclei followed by counting of the DAPI-labeled structures. Confocal fluorescence images were recorded with a Zeiss LSM980 confocal microscope using a 20X objective lens by Z-stack scanning. 3D images are reconstructed using Z-stack files, and cell counting was performed on three-dimensional reconstructed tubule images using IMARIS Scientific Image Processing & Analysis software (v10.2.0, Bitplane, Zurich, Switzerland). Counting was automated using IMARIS "spot analysis" for nuclei. DAPI fluorescence was quantified to assess relative DNA abundances in individual nuclei, allowing construction of histograms of DAPI fluorescence intensity to assess relative DNA amounts in each nucleus. The DAPI-labeled microdissected CCDs were also labeled with anti-AQP2 (rabbit, 1:500, Knepper Lab, #K5007) followed by a secondary antibody (Alexa Fluor 568 goat anti-rabbit). IMARIS was used to quantify the diameter and cross-sectional area of the microdissected tubules.

Glomerular counts in wild-type (WT) and Ser552Ala mutant mice. Whole kidney glomerular counts were done using the acid maceration method of Damidian *et al*.[46] as modified by Peterson *et al*.[47] Briefly, a mouse kidney was chopped into small pieces and then reduced to a suspension consisting of glomeruli and small renal tubule fragments by incubation in 6M HCl at 37 °C for 90 minutes. Glomeruli (identified by their round shape) were counted in triplicate in three aliquots of the total suspension under a Wild M8 dissection stereomicroscope and total glomerular number was calculated by multiplying by the ratio of the total volume to the aliquot-volume.

Preparation of nuclear fractions. Manually dissected inner medullas were transferred to a BeadBug™ tube prefilled with 3 mm Zicronium beads (Millipore Sigma, # Z763802-50EA) and homogenized (BeadBug™ 6, Benchmark Scientific, 3000rpm, 30 sec, 3 cycles) with 150-180 µL of lysis

buffer (250 mM sucrose, 10 nM triethanolamine, pH = 7.6). Nuclear fractions were extracted by NE-PER nuclear and cytoplasmic extraction reagents (Thermo Scientific, # 78833), following the manufacturer's instructions. Immunoblot analysis was used to assess the adequacy of nuclear purification by measuring Lamin A/C (rabbit, 1:1000, Cell signaling # 2032, a nuclear protein).

Immunocytochemistry of kidney sections. Mice underwent cervical dislocation and were immediately perfused via the left ventricle of the heart with ice-cold DPBS followed by 4% paraformaldehyde in DPBS. The kidneys were post-fixed in 4% paraformaldehyde solution, further processed with alcohol and xylene, and then embedded in paraffin blocks. 5 µm sections were mounted on glass slides for immunofluorescence staining. For dewaxing, the tissue sections were immersed in xylene, then gradually rehydrated by using decreasing concentrations of ethanol (100%, 100%, 95%, and 70%). After performing antigen retrieval using the antigen retrieval buffer (Elabscience, #E-IR-R220A), the tissue sections were permeabilized for 20 minutes with permeabilization buffer (PBS with 0.3% Triton X-100 and 0.1% BSA). Tissue sections were then blocked for 30 minutes with blocking buffer (PBS with 1% BSA and 0.2% gelatin). Primary antibodies were applied overnight at 4°C. The secondary antibody incubation was carried out for 1 hour at room temperature. Immunofluorescent labeling was analyzed using a Zeiss LSM980 confocal microscope using ZENBlue software (Zeiss). The primary and secondary antibodies are listed in the legends.

Determination of nephron:CCD ratio in mice. In mice and other mammals, multiple nephrons converge to form a single CCD in the cortical labyrinth via branching of CNTs and iCTs.[48] The ratio of medullary thick ascending limb (MTAL) to OMCD provides a measure of cortical branching ratio (nephrons : CCD) because all structures between the MTAL and OMCD other than the CNT and iCT are unbranched (MTAL, cortical thick ascending limb, CCD in the medullary rays and OMCD).[49]

To measure the MTAL/OMCD ratio, kidneys from WT and Ser552Ala mutant mice underwent perfusion fixation and embedding as described in the previous paragraph. Tissue sectioning was performed to obtain cross-sections of the inner stripe of the outer medulla perpendicular to the corticomedullary axis. The sections underwent immunofluorescence labeling for the Na-K-2Cl cotransporter NKCC2 (a marker for the MTAL) and for AQP2 (a marker for OMCD). After immunofluorescence staining, MTALs and OMCDs were counted in demarcated square fields.

Small-sample RNA-seq in microdissected CCDs. For RNA-seq analyses, four to eight CCDs were collected for each sample for a total length of 1.5-3.0 mm. mRNA collection and purification were performed by using a Direct-Zol RNA MicroPrep kit (Zymo Research, Irvine, CA). cDNA was generated using the SMART-Seq V4 Ultra Low RNA Kit (Takara Bio, Mountain View, CA). After 14 cycles of amplification, 1 ng of cDNA was "tagmented" and bar coded using a Nextera XT DNA Sample Preparation Kit (Illumina, #FC-131-1024). The final libraries were purified using AmPure XP magnetic beads (Beckman Coulter, Indianapolis, IN) and quantified using a Qubit 2.0 Fluorometer (Thermo Fisher Scientific, Waltham, MA). Sample quantity and quality were assayed on an Agilent 2100 bioanalyzer. cDNA library concentrations were normalized, and samples were pooled and sequenced on an Illumina Novaseq 6000 platform using a 50 bp paired-end modality. FastQC was used to evaluate sequence quality (software version 0.11.9). Adapter contamination was not significant, so read trimming was not performed. RNA-seq reads were indexed using STAR (2.7.6a) and aligned to the mouse reference genome from *Ensembl* (release 104) with the matching genome annotation file (release 104).[50] Default settings were used except for:–runThreadN $SLURM_CPUS_PER_TASK –outFilterMismatchNmax 3 –outSAMstrandField intronMotif –alignIntronMax 1000000 –alignMatesGapMax 1000000 --outFilterIntronMotifs RemoveNoncanonicalUnannotated –outFilterMultimapNmax 1. Transcripts per million (TPM) and expected read counts were generated using RSEM (1.3.3).[51] Unless otherwise

specified, the computational analyses were performed on the NIH Biowulf High-Performance Computing platform.

Results

PKA phosphorylates β-catenin at Ser552 in response to vasopressin. Vasopressin increases phosphorylation of β-catenin at Ser552, a putative PKA-target site.[24, 52] To confirm this effect and to address whether PKA mediates the increase, we carried out initial studies in cultured mpkCCD cells (**Figure 2**). We found that phosphorylation of β-catenin at Ser552 was increased within 30 minutes of desmopressin (dDAVP) addition, but that another putative PKA target site in β-catenin, Ser675 did not undergo a change in phosphorylation (**Figure 2A**).[53] (Shorter time points were previously studied using protein mass spectrometry in native inner medullary collecting duct (IMCD) cells and these studies showed that Ser552 phosphorylation increased within 5 minutes of exposure to dDAVP.[54]) The effect on Ser552 phosphorylation was sustained for 60 minutes, but diminished over time after 60 minutes in mpkCCD cells (**Figure 2B**). AQP2 abundance was increased, but required 12 to 24 hours of dDAVP exposure (**Figure 2A**). PKA deletion strongly decreased Ser552 phosphorylation in both the presence and absence of dDAVP, while it had no effect on Ser675 phosphorylation (**Figure 2C,D**). As previously observed, PKA deletion resulted in a marked decrease in AQP2 abundance. Western blots using an antibody that recognizes proteins phosphorylated in an R-R-X-p(S/T) motif, characteristic of PKA-mediated phosphorylation, showed a marked decrease with PKA deletion. These results demonstrate a role of PKA in the phosphorylation of β-catenin at Ser552 in response to dDAVP.

CRISPR-mediated mutation of Ser552 of β-catenin in mouse. To investigate the role of β-catenin phosphorylation at Ser552 in native collecting ducts, we generated a *Ctnnb1* Ser552Ala knock-in mutant mouse line using CRISPR/Cas9 (**Figure 3A**). Because the neighboring threonine has sometimes been reported to be phosphorylated,[24] we also mutated Thr551 to Ala in the same animals, although we will refer to these mice as Ser552Ala knock-in mutant mice in what follows for simplicity. We found that the homozygous mutant mice survived and appeared superficially indistinguishable from WT mice, unlike the global β-catenin-knockout in mice, which is lethal before gastrulation.[55] The absence of

Ser552 phosphorylated β-catenin was confirmed in homozygotes (Ho), and phosphorylation was reduced in heterozygotes (Het) (**Figure 3B**). **Figure 3C** shows immunoblots of the nuclear fractions of the inner medullas of mice showing that the homozygous mutant mice displayed no phosphorylated β-catenin, while total nuclear β-catenin was unaffected (**Figure 3D**). The latter observation demonstrates that the mutation does not prevent translocation of β-catenin into the nucleus. **Figure 3E** shows random daytime urinary osmolalities for WT and Ser552Ala mutant mice indicating that the Ser552Ala mutant mice are capable of concentrating urine to more than 7 times the plasma level (plasma osmolality: ~300 mOsm/kgH_2O) even without water restriction or vasopressin administration. **Figure 3F** shows immunofluorescence labeling of ZO-1 and Na^+-K^+-ATPase (ATP1A1) in microdissected CCDs in WT and Ser552Ala mutant mice showing no major changes in distribution of these two polarity markers.

A broad survey of 33 tissues and organs, including gross morphology and histology, revealed no gross structural abnormalities in the Ser552Ala mutant mice (Supplementary Spreadsheet PathSurveyData.xlsx at https://esbl.nhlbi.nih.gov/Databases/Catenin-RNA-seq/Data/). Analysis of blood samples revealed no abnormalities of serum glucose, creatinine, urea, calcium, inorganic phosphorus, total protein, albumin, bilirubin, cholesterol, triglycerides, alkaline phosphatase, creatine kinase, alanine transaminase, aspartate aminotransferase, or lactate dehydrogenase (PathSurveyData.xlsx at https://esbl.nhlbi.nih.gov/Databases/Catenin-RNA-seq/Data/) In addition, there were no abnormalities of any hematologic parameter or the blood smear (PathSurveyData.xlsx at https://esbl.nhlbi.nih.gov/Databases/Catenin-RNA-seq/Data/).

Glomerular counts. Direct counts of the number of glomeruli per kidney showed no differences (13600 ± 1015 per kidney [n=3] in WT versus 13500 ± 889 per kidney [n=3] in Ser552Ala mutant mice, *P* = 0.904, NS), consistent with the conclusion that the number of nephrons was unchanged in Ser552Ala mutant mice. This finding fits with the observation that kidney weight normalized to body weight was

not different between WT mice (0.0126±0.0004 [n=3]) and Ser552Ala mutant mice (0.0126±0.0004 [n=3]).

Quantification of cortical renal tubule branching in WT versus Ser552Ala mutant mice. β-catenin and the *Wnt* signaling pathway are important determinants of collecting duct branching during development.[30-32] In the adult mammalian kidney, the endpoint of developmental branching in the cortex are the CNTs, including the CNT and iCTs, both of which are found in the cortical labyrinth. The CNT and iCTs are the only branched tubule segments prior to the IMCDs.[49] Branched CNTs and iCTs constitute a manifold-like structure in which several nephrons converge to a single CCD. In rat, on average, slightly greater than 5 nephrons merge to form one CCD.[56] A similar converging structure is present in the mouse and the nephron:CCD ratio for mouse has been reported to be between 5 and 7.[48] **Figure 4A** shows a typical cortical branched structure microdissected from a mouse and labeled with antibodies recognizing Na^+-K^+-ATPase (ATP1A1) (green), the thiazide sensitive Na^+-Cl^- cotransporter (SLC12A3) (purple) and parvalbumin (PVALB) (cyan). SLC12A3 and PVALB mark multiple distal convoluted tubules (DCTs) that converge into a single CCD via CNTs/iCTs.

To measure the cortical branching ratio (nephron:CCD) in WT versus Ser552Ala mutant mice, we used a variant of the technique of Knepper *et al*.[56] to quantify the MTAL:OMCD ratio in the inner stripe of the outer medulla. The MTAL:OMCD ratio is a measure of the average number of cortical branches because the other segments between the MTAL and OMCD are unbranched (**Figure 4B**). To measure the MTAL:OMCD ratio, MTALs and OMCDs are counted in random fields from histological sections taken perpendicular to the corticomedullary axis in the inner stripe of the outer medulla. To identify these segments unequivocally, we labeled the MTALs using an antibody to the bumetanide-sensitive Na^+-K^+-$2Cl^-$ cotransporter (NKCC2) (green) and OMCDs with an antibody to AQP2 (red). **Figure 4C and D** show representative fields from WT and Ser552Ala mutant mice, respectively. The measured MTAL:OMCD ratio was significantly greater in the WT mice (6.18 ± 0.66) than in the Ser552Ala mutant mice (3.33 ±

0.82) (**Figure 4E**). This indicates that cortical branching in Ser552Ala mutant mice is attenuated. We asked whether the MTAL:OMCD ratio was different because of a difference in the number of MTALs or the number of OMCDs. The number of MTALs per unit cross sectional area was found to be the same for the two genotypes (**Figure 4F**), consistent with our prior conclusion that the Ser552Ala mutant mice and WT mice have the same number of nephrons based on glomerular counting. In contrast, the number of OMCDs per unit cross sectional area was much higher in the kidneys of Ser552Ala mutant mice (**Figure 4G**). Thus, there are approximately the same number of nephrons in WT versus Ser552Ala mutant mice (consistent with glomerular counting data), but that a difference in branching at the level of the CNTs/iCTs translates to a greater number of collecting ducts in the outer medulla and medullary rays of the cortex. An additional observation from **Figure 4C&D** is that the OMCDs appear to have smaller diameters in the Ser552Ala mutant mice than in the WT mice. To address this observation quantitatively, we used morphometry of the labeled sections to determine the average diameter and cross-sectional area of MTALs and OMCD (**Figure 4-H&I**). As shown in **Figure 4H**, both the diameter and cross-sectional area of OMCDs were significantly lower in Ser552Ala mutant mice versus WT controls. In contrast, there was no difference between WT and Ser552Ala mutant mice with regard to diameter and cross-sectional area of MTALs (**Figure 4I**).

Effect of Ser552Ala mutation on IMCDs of renal papilla. Figure 5A shows longitudinal sections of papillae from a WT mouse and a Ser552Ala mutant mouse. Ser552Ala mutant mice appeared to have a greater number of collecting ducts with smaller diameters. In separate mice, the papilla was cross sectioned at approximately 25 µm (upper panels) and 75 µm (lower panels) from the papillary tip (**Figure 5B**) to quantify the differences. **Figure 5C** summarizes total IMCD numbers from the end of the tip. At 25 µm, there was no significant difference in the number of IMCDs between WT (6.67 $\pm$ 0.58, n=3]) and Ser552Ala mutant mice (6.33 $\pm$ 0.58, n=3, P = 0.519, NS), indicating that the numbers of duct of Bellini orifices were not likely to be different (**Figure 5C**). However, the number of IMCDs was greater

in Ser552Ala mutant mice than in WT mice at a higher level of the papilla (75 µm or 125 µm from the end, **Figure 5C**).

Effect of Ser552Ala mutation on the CCD transcriptome. The foregoing experiments demonstrated substantial effects of the Ser552Ala β-catenin mutation on the size and number of collecting ducts. Since β-catenin functions as a transcriptional co-regulator, we asked whether CCDs from adult Ser552Ala mice manifest changes in gene expression as measured by RNA-seq. We carried out RNA-seq in microdissected CCDs from Ser552Ala mutant and WT mice that were otherwise untreated. The CCD samples were analyzed for each of four wild-type mice (n=4 biological replicates) and each of four Ser552Ala mutant mice (n=4 biological replicates) (**Figure 6**). The full curated data set is available at https://esbl.nhlbi.nih.gov/Databases/Catenin-RNA-seq/. Raw data deposited at GEO (https://www.ncbi.nlm.nih.gov/geo/query/acc.cgi?acc=GSE291074, Secure token: yvaresyoxrmlfaf).

Out of 13,746 transcripts with mean TPM greater than 1 in WT, 42 were identified as increased in S552A mutant CCDs and 64 were identified as decreased based on dual criteria ($|\log_2[\text{Ser552Ala/WT}]| > 0.60$ and $P < 0.05$). (The threshold of 0.60 was calculated from the entire population of $\log_2$[Ser552Ala/WT] values to approximate the 95% confidence interval using the Empirical Bayes' Method.[57]). Gene set enrichment analysis revealed that upregulated transcripts mapped highly significantly to *Gene Ontology Biological Process* terms related to cell division ($P < 10^{-6}$) including "mitotic cell cycle process", "mitotic cytokinesis", "nuclear division", "spindle organization", "G2/M transition of mitotic cell cycle", and "regulation of cell cycle process" (**Table 1A**). Control analysis using 42 randomly selected genes revealed no *Biological Process* terms with Fisher Exact P values less than 1.3×10^{-2}. Transcripts associated with the *Gene Ontology Biological Process* term "mitotic cell cycle process" are labeled on the right-hand side of **Figure 6**. Among the "mitotic cell cycle process" gene set elements are four key protein kinases involved in cell cycle regulation and mitosis, aurora kinase B (*Aurkb*), cyclin-dependent kinase 1 (*Cdk1*), NIMA-related expressed kinase 5 (*Nek5*), and polo-like kinase 1 (*Plk1*).

Interestingly, one of the upregulated transcripts codes for the transcription factor *Foxm1* (also known as "*Trident*"), a key regulator of the expression of cell cycle genes essential for DNA replication and mitosis.[58-60]

Gene set enrichment analysis with the down-regulated transcripts mapped significantly to only one *Gene Ontology Biological Process* term: "animal organ development" (**Table 1B**) (transcripts labeled on left-hand side of **Figure 6**). Control analysis using 64 randomly selected genes revealed no *Biological Process* terms with Fisher Exact *P* values less than 5.8×10^{-3}. Among the downregulated transcripts in the CCD of mice with the Ser552Ala mutation in β-catenin were two cyclin-dependent kinase inhibitor proteins (*Cdkn1b* and *Cdk1c*), which are negative regulators of cell cycle progression and proliferation.[61, 62] Aside from *Cdkn1b* and *Cdkn1c* mRNAs, a number of transcripts that code for proteins involved in regulation of transcription were decreased in abundance, including transcription factors (*Cebpd*, *Nfix*, *Zfp704*), transcriptional coregulators (*Mta1*, *Tada2b*, *Tshz1*, *Zfpm1*), regulators of histone acetylation (*Anp32a* and *Brd1*), and a protein kinase with a key role in Wnt/β-catenin signaling (*Csnk2a2*) (**Figure 6**).

Despite the induction of several transcripts involved in the cell cycle, there was no evidence of dedifferentiation as shown in **Table 2,** indicating that the abundances of receptors, water channels, potassium channels and sodium channels characteristic of differentiated collecting duct principal cells were unaffected by the Ser552Ala mutation. Notably, the Ser552Ala mutation did not significantly affect the abundance of the transcript coding for AQP2.

Although the single-tubule RNA-seq in CCDs demonstrated a pattern of expression changes that point to a possible role for β-catenin phosphorylation at Ser552 to inhibit cellular proliferation, it is not clear whether these transcriptional changes are accompanied by overt cell proliferation or alternatively are associated with entry into the cell cycle with cell cycle arrest. To address these possibilities in the CCD, we carried out DAPI labeling of microdissected CCDs from Ser552Ala mutant mice and wild type mice (**Figure 7A**). The number of cells per unit length determined by counting DAPI-labeled nuclei was

not significantly different between WT and Ser552Ala mutant mice (**Figure 7B**). However, as seen previously for OMCDs, the diameters of CCDs from Ser552Ala mutant mice were significantly smaller than in CCDs from WT mice (**Figure 7C**). DNA content in nuclei can be assessed by measuring DAPI fluorescence intensity integrated over the entire nucleus. We expect nuclear DNA content to increase in S phase and to be maintained in G2 phase and early M phase. **Figure 7D** shows a histogram of nuclear DAPI levels. The mean per-nucleus DAPI fluorescence is higher in Ser552Ala mutant mice compared to WT mice (162.3 $\pm$ 46.8 [n=4] vs 150.8 $\pm$ 42.6 [n=4], P = 0.005). Nuclei with total DAPI fluorescence greater than the indicated threshold (mean plus one standard deviation of total fluorescence) were classified as high-intensity nuclei. The proportion of cells with high-intensity nuclei was statistically significantly higher in Ser552Ala mutant mice compared to WT mice (26.7% *vs*. 13.8%, P = 0.0005, Fisher exact test). Overall, the DAPI fluorescence data is consistent with a lack of overt cellular proliferation, but the increase in cells with high intensity DAPI fluorescence is consistent with a higher frequency of cells arrested in G2/M.

Discussion

In the adult mouse kidney, branching is seen only in the cortical labyrinth and inner medulla, but not in the collecting ducts of the cortical medullary rays (CCDs) or of the outer medulla (OMCDs) (**Introduction**). The CCDs and OMCDs are long unbranched segments that form by inter-branch elongation starting at gestational age 15.5.[33] Our data indicate that, in total, there are 11 generations of dichotomous branches (calculated as $\log_2[13600/6.3]$ from **Figure 8**) in the collecting duct system of normal WT mice, consistent with the findings of Cebrián *et al*.[33] The β-catenin Ser552Ala mutant mice also have 11 generations of dichotomous branches, but they are divided differently between the cortical labyrinth (fewer in mutant) and inner medulla (more in mutant). Within the branching architecture, the long unbranched OMCD/CCD occurs at average generation level 8.4 ($\log_2[2200/6.3]$ from **Figure 8**) in the WT mice and at average generation level 9.2 ($\log_2[4100/6.7]$) in the Ser552Ala mutant mice. Thus, it appears that the timing of collecting duct branching versus collecting duct elongation is altered by the Ser552Ala mutation. Because elongation occurs higher up in the branched tree of the collecting duct system, there are more OMCDs and CCDs in the Ser552Ala mutant mice than in WT mice, which if other factors were equal would predict more overall transport of sodium, potassium and water. However, we found that these collecting ducts have, on average, smaller diameters. The smaller diameters may compensate for the larger collecting duct counts with regard to total luminal surface area available for transport.

To address the mechanisms that govern the timing between collecting duct branching and elongation, extensive additional studies will be needed to address two questions: 1) What are the signals that are responsible for local elongation of collecting ducts in the developing outer medulla and cortical medullary rays?; and 2) How is the rate of branching controlled and eventually stopped in the immediate post-natal period? As reviewed in the **Introduction**, collecting ducts first acquire vasopressin sensitivity in the perinatal period, which overlaps the final stages of collecting duct

branching and collecting duct elongation. Thus, vasopressin signaling, involving β-catenin phosphorylation, is quite possibly a determinant of collecting duct branching architecture through effects on collecting duct branching and/or elongation. Wnt signaling via Wnt7b and β-catenin are important for elongation of the renal medulla as a whole including the loop of Henle,[63] and we note that vasopressin also markedly increases β-catenin phosphorylation at Ser552 in the medullary thick ascending limb of rat.[64]

The effect of the β-catenin Ser552Ala mutation on gene expression in adult CCDs (RNA-seq) is relatively subtle, with selective changes in transcripts involved in regulation of cell cycle and organ development (**Table 1**). However, cell counts per unit length of collecting ducts showed no significant changes. The increase in mean DNA content and in the number of high DNA-content cells (**Figure 7D**) is consistent with the possibility that there are more collecting duct cells in the cell cycle, but with G2/M arrest rather than frank proliferation. Among the transcripts decreased in abundance in the mutant CCDs were two cyclin-dependent kinase inhibitor proteins (Cdkn1b and Cdk1c), which are negative regulators of cell cycle progression and proliferation.[61, 62] *Cdkn1b* is known as p27 (or Kip1), while *Cdkn1c* is known as p57 (or Kip2). They both work by inhibiting the cyclin E-CDK2 and cyclin D-CDK4/6 complexes. p27 and p57 are related to *Cdkn1a* (p21), which is involved in a phenomenon known as 'cell senescence'. However, p27 and p57 are not thought to be involved in this phenomenon. *Cdkn1b*/p27 is instead involved in regulation of cell 'quiescence'.[65] Cell quiescence is a reversible state in which cells exit the cell cycle (G0 phase) and maintain functional differentiation. Quiescent cells, unlike senescent cells, can be induced to re-enter the cell cycle and resume proliferation.[66] *Cdkn1c*/p57 has a special role in development, and is essential for proper organogenesis.[67-69]

A topic for future studies is the mechanism by which β-catenin phosphorylation at Ser552 may alter gene expression. A clue is offered by the data of Takemaru and Moon[70] showing that Armadillo domain 10, which contains Ser552, is the site of p300 or CREB-binding protein (CBP) binding to β-catenin

(**Figure 1**). CBP and p300 are histone acetyltransferases that alter chromatin structure and increase local DNA accessibility. Thus, it appears possible that transcription may be altered by Ser552 phosphorylation as a consequence of altered CBP- or p300-mediated changes in the chromatin structure surrounding target genes.

DISCLOSURES

The authors declare no conflicting financial interests.

FUNDING

The work was funded by the Division of Intramural Research, National Heart, Lung, and Blood Institute (project ZIA-HL001285 and ZIA-HL006129, M.A.K.).

ACKNOWLEDGEMENTS

The authors thank Dr. Chengyu Liu and Dr. Fan Zhang (NHLBI Transgenic Core) for creating the mutant mice. Next-generation sequencing was done in the NHLBI DNA Sequencing Core Facility (Yuesheng Li, Director). Light microscopy images were taken in the NHLBI Confocal Microscopy Core Facility (Dr. Christian Combs, Director). Dr. Matthew Starost carried out pathological surveys of mouse phenotype. Computational analyses were performed on the NIH Biowulf High-Performance Computing platform.

DATA SHARING

Curated RNA-seq data are accessible at https://esbl.nhlbi.nih.gov/Databases/Catenin-RNA-seq/.

Sequencing data (FASTQ) have been deposited in the GEO:
https://www.ncbi.nlm.nih.gov/geo/query/acc.cgi?acc=GSE291074 (Secure token: yvaresyoxrmlfaf).

REFERENCES

1. Sandoval PC, Claxton JS, Lee JW, Saeed F, Hoffert JD, Knepper MA: Systems-level analysis reveals selective regulation of Aqp2 gene expression by vasopressin. *Scientific reports,* 6**:** 34863, 2016 10.1038/srep34863

2. Hasler U, Leroy V, Martin PY, Feraille E: Aquaporin-2 abundance in the renal collecting duct: new insights from cultured cell models. *American journal of physiology Renal physiology,* 297**:** F10-18, 2009 10.1152/ajprenal.00053.2009

3. Nedvetsky PI, Tabor V, Tamma G, Beulshausen S, Skroblin P, Kirschner A, et al.: Reciprocal regulation of aquaporin-2 abundance and degradation by protein kinase A and p38-MAP kinase. *Journal of the American Society of Nephrology : JASN,* 21**:** 1645-1656, 2010 10.1681/ASN.2009111190

4. Sandoval PC, Slentz DH, Pisitkun T, Saeed F, Hoffert JD, Knepper MA: Proteome-wide measurement of protein half-lives and translation rates in vasopressin-sensitive collecting duct cells. *Journal of the American Society of Nephrology : JASN,* 24**:** 1793-1805, 2013 10.1681/ASN.2013030279

5. Ganote CE, Grantham JJ, Moses HL, Burg MB, Orloff J: Ultrastructural studies of vasopressin effect on isolated perfused renal collecting tubules of the rabbit. *The Journal of cell biology,* 36**:** 355-367, 1968 10.1083/jcb.36.2.355

6. Kirk KL, DiBona DR, Schafer JA: Morphologic response of the rabbit cortical collecting tubule to peritubular hypotonicity: quantitative examination with differential interference contrast microscopy. *J Membr Biol,* 79**:** 53-64, 1984 10.1007/BF01868526

7. Nielsen S, Muller J, Knepper MA: Vasopressin- and cAMP-induced changes in ultrastructure of isolated perfused inner medullary collecting ducts. *Am J Physiol,* 265**:** F225-238, 1993 10.1152/ajprenal.1993.265.2.F225

8. Chou CL, Yu MJ, Kassai EM, Morris RG, Hoffert JD, Wall SM, et al.: Roles of basolateral solute uptake via NKCC1 and of myosin II in vasopressin-induced cell swelling in inner medullary collecting duct. *American journal of physiology Renal physiology,* 295**:** F192-201, 2008 10.1152/ajprenal.00011.2008

9. Nielsen S, Chou CL, Marples D, Christensen EI, Kishore BK, Knepper MA: Vasopressin increases water permeability of kidney collecting duct by inducing translocation of aquaporin-CD water channels to plasma membrane. *Proceedings of the National Academy of Sciences of the United States of America,* 92**:** 1013-1017, 1995 10.1073/pnas.92.4.1013

10. Nielsen S, Knepper MA: Vasopressin activates collecting duct urea transporters and water channels by distinct physical processes. *Am J Physiol,* 265**:** F204-213, 1993 10.1152/ajprenal.1993.265.2.F204

11. Nunes P, Hasler U, McKee M, Lu HA, Bouley R, Brown D: A fluorimetry-based ssYFP secretion assay to monitor vasopressin-induced exocytosis in LLC-PK1 cells expressing aquaporin-2. *Am J Physiol Cell Physiol,* 295**:** C1476-1487, 2008 10.1152/ajpcell.00344.2008

12. Brown D: The ins and outs of aquaporin-2 trafficking. *American journal of physiology Renal physiology,* 284**:** F893-901, 2003 10.1152/ajprenal.00387.2002

13. Tomita K, Pisano JJ, Knepper MA: Control of sodium and potassium transport in the cortical collecting duct of the rat. Effects of bradykinin, vasopressin, and deoxycorticosterone. *The Journal of clinical investigation,* 76**:** 132-136, 1985 10.1172/JCI111935

14. Reif MC, Troutman SL, Schafer JA: Sodium transport by rat cortical collecting tubule. Effects of vasopressin and desoxycorticosterone. *The Journal of clinical investigation,* 77**:** 1291-1298, 1986 10.1172/JCI112433

15. Simon H, Gao Y, Franki N, Hays RM: Vasopressin depolymerizes apical F-actin in rat inner medullary collecting duct. *Am J Physiol,* 265**:** C757-762, 1993 10.1152/ajpcell.1993.265.3.C757

16. Tamma G, Klussmann E, Maric K, Aktories K, Svelto M, Rosenthal W, et al.: Rho inhibits cAMP-induced translocation of aquaporin-2 into the apical membrane of renal cells. *American journal of physiology Renal physiology,* 281**:** F1092-1101, 2001 10.1152/ajprenal.0091.2001

17. Chou CL, Christensen BM, Frische S, Vorum H, Desai RA, Hoffert JD, et al.: Non-muscle myosin II and myosin light chain kinase are downstream targets for vasopressin signaling in the renal collecting duct. *The Journal of biological chemistry,* 279**:** 49026-49035, 2004 10.1074/jbc.M408565200

18. Noda Y, Horikawa S, Kanda E, Yamashita M, Meng H, Eto K, et al.: Reciprocal interaction with G-actin and tropomyosin is essential for aquaporin-2 trafficking. *The Journal of cell biology,* 182**:** 587-601, 2008 10.1083/jcb.200709177

19. Loo CS, Chen CW, Wang PJ, Chen PY, Lin SY, Khoo KH, et al.: Quantitative apical membrane proteomics reveals vasopressin-induced actin dynamics in collecting duct cells. *Proceedings of the National Academy of Sciences of the United States of America,* 110**:** 17119-17124, 2013 10.1073/pnas.1309219110

20. Miller RL, Sandoval PC, Pisitkun T, Knepper MA, Hoffert JD: Vasopressin inhibits apoptosis in renal collecting duct cells. *American journal of physiology Renal physiology,* 304**:** F177-188, 2013 10.1152/ajprenal.00431.2012

21. Ando F: Activation of AQP2 water channels by protein kinase A: therapeutic strategies for congenital nephrogenic diabetes insipidus. *Clin Exp Nephrol,* 25**:** 1051-1056, 2021 10.1007/s10157-021-02108-6

22. Olesen ETB, Fenton RA: Aquaporin 2 regulation: implications for water balance and polycystic kidney diseases. *Nature reviews Nephrology,* 17**:** 765-781, 2021 10.1038/s41581-021-00447-x

23. Salhadar K, Matthews A, Raghuram V, Limbutara K, Yang CR, Datta A, et al.: Phosphoproteomic Identification of Vasopressin/cAMP/Protein Kinase A-Dependent Signaling in Kidney. *Mol Pharmacol,* 99**:** 358-369, 2021 10.1124/mol.120.119602

24. Park E, Yang CR, Raghuram V, Deshpande V, Datta A, Poll BG, et al.: Data resource: vasopressin-regulated protein phosphorylation sites in the collecting duct. *American journal of physiology Renal physiology,* 324**:** F43-F55, 2023 10.1152/ajprenal.00229.2022

25. Pisitkun T, Hoffert JD, Saeed F, Knepper MA: NHLBI-AbDesigner: an online tool for design of peptide-directed antibodies. *Am J Physiol Cell Physiol,* 302**:** C154-164, 2012 10.1152/ajpcell.00325.2011

26. Kyte J, Doolittle RF: A simple method for displaying the hydropathic character of a protein. *J Mol Biol,* 157**:** 105-132, 1982 10.1016/0022-2836(82)90515-0

27. Kanamori M, Sandy P, Marzinotto S, Benetti R, Kai C, Hayashizaki Y, et al.: The PDZ protein tax-interacting protein-1 inhibits beta-catenin transcriptional activity and growth of colorectal cancer cells. *The Journal of biological chemistry,* 278**:** 38758-38764, 2003 10.1074/jbc.M306324200

28. Rinschen MM, Yu MJ, Wang G, Boja ES, Hoffert JD, Pisitkun T, et al.: Quantitative phosphoproteomic analysis reveals vasopressin V2-receptor-dependent signaling pathways in renal collecting duct cells. *Proceedings of the National Academy of Sciences of the United States of America,* 107**:** 3882-3887, 2010 10.1073/pnas.0910646107

29. Bansal AD, Hoffert JD, Pisitkun T, Hwang S, Chou CL, Boja ES, et al.: Phosphoproteomic profiling reveals vasopressin-regulated phosphorylation sites in collecting duct. *Journal of the American Society of Nephrology : JASN,* 21**:** 303-315, 2010 10.1681/ASN.2009070728

30. Iglesias DM, Hueber PA, Chu L, Campbell R, Patenaude AM, Dziarmaga AJ, et al.: Canonical WNT signaling during kidney development. *American journal of physiology Renal physiology,* 293**:** F494-500, 2007 10.1152/ajprenal.00416.2006

31. Marose TD, Merkel CE, McMahon AP, Carroll TJ: Beta-catenin is necessary to keep cells of ureteric bud/Wolffian duct epithelium in a precursor state. *Dev Biol,* 314**:** 112-126, 2008 10.1016/j.ydbio.2007.11.016

32. Bridgewater D, Cox B, Cain J, Lau A, Athaide V, Gill PS, et al.: Canonical WNT/beta-catenin signaling is required for ureteric branching. *Dev Biol,* 317**:** 83-94, 2008 10.1016/j.ydbio.2008.02.010

33. Cebrian C, Borodo K, Charles N, Herzlinger DA: Morphometric index of the developing murine kidney. *Dev Dyn,* 231**:** 601-608, 2004 10.1002/dvdy.20143

34. Peter K: Untersuchungen über Bau und Entwicklung der Niere. Jena, Germany: Fisher. 1909.

35. Oliver J: Nephrons and Kidneys: A Quantitative Study of Developmental and Evolutionary Mammalian Renal Architectonics. Chapter 14 (Configuration of the Complete Collecting System in the Adult Kidney). Harper and Row, New York;1968.

36. Short KM, Combes AN, Lefevre J, Ju AL, Georgas KM, Lamberton T, et al.: Global quantification of tissue dynamics in the developing mouse kidney. *Dev Cell,* 29**:** 188-202, 2014 10.1016/j.devcel.2014.02.017

37. Knepper MA: Urea transport in nephron segments from medullary rays of rabbits. *Am J Physiol,* 244**:** F622-627, 1983 10.1152/ajprenal.1983.244.6.F622

38. Knepper MA: Urea transport in isolated thick ascending limbs and collecting ducts from rats. *Am J Physiol,* 245**:** F634-639, 1983 10.1152/ajprenal.1983.245.5.F634

39. Royaux IE, Wall SM, Karniski LP, Everett LA, Suzuki K, Knepper MA, et al.: Pendrin, encoded by the Pendred syndrome gene, resides in the apical region of renal intercalated cells and mediates bicarbonate secretion. *Proceedings of the National Academy of Sciences of the United States of America,* 98**:** 4221-4226, 2001 10.1073/pnas.071516798

40. Rajerison RM, Butlen D, Jard S: Ontogenic development of antidiuretic hormone receptors in rat kidney: comparison of hormonal binding and adenylate cyclase activation. *Mol Cell Endocrinol,* 4**:** 271-285, 1976 10.1016/0303-7207(76)90061-7

41. Bonilla-Felix M, Jiang W: Aquaporin-2 in the immature rat: expression, regulation, and trafficking. *Journal of the American Society of Nephrology : JASN,* 8**:** 1502-1509, 1997 10.1681/ASN.V8101502

42. Isobe K, Jung HJ, Yang CR, Claxton J, Sandoval P, Burg MB, et al.: Systems-level identification of PKA-dependent signaling in epithelial cells. *Proceedings of the National Academy of Sciences of the United States of America,* 114**:** E8875-E8884, 2017 10.1073/pnas.1709123114

43. Chou CL, Limbutara K, Kao AR, Clark JZ, Nein EH, Raghuram V, et al.: Collecting duct water permeability inhibition by EGF is associated with decreased cAMP, PKA activity, and AQP2 phosphorylation at Ser(269). *American journal of physiology Renal physiology,* 326**:** F545-F559, 2024 10.1152/ajprenal.00197.2023

44. Park E, Yang CR, Raghuram V, Chen L, Chou CL, Knepper MA: Using CRISPR-Cas9/phosphoproteomics to identify substrates of calcium/calmodulin-dependent kinase 2delta. *The Journal of biological chemistry,* 299**:** 105371, 2023 10.1016/j.jbc.2023.105371

45. Pisitkun T, Bieniek J, Tchapyjnikov D, Wang G, Wu WW, Shen RF, et al.: High-throughput identification of IMCD proteins using LC-MS/MS. *Physiol Genomics,* 25**:** 263-276, 2006 10.1152/physiolgenomics.00214.2005

46. Damadian RV, Shwayri E, Bricker NS: On the Existence of Non-Urine Forming Nephrons in the Diseased Kidney of the Dog. *J Lab Clin Med,* 65**:** 26-39, 1965

47. Peterson SM, Wang X, Johnson AC, Coate ID, Garrett MR, Didion SP: Estimation of Nephron Number in Whole Kidney using the Acid Maceration Method. *J Vis Exp*, 2019 10.3791/58599

48. Zhai XY, Thomsen JS, Birn H, Kristoffersen IB, Andreasen A, Christensen EI: Three-dimensional reconstruction of the mouse nephron. *Journal of the American Society of Nephrology : JASN,* 17**:** 77-88, 2006 10.1681/ASN.2005080796

49. Christensen EI, Wagner CA, Kaissling B: Uriniferous tubule: structural and functional organization. *Comprehensive Physiology,* 2**:** 805-861, 2012 10.1002/cphy.c100073

50. Dobin A, Davis CA, Schlesinger F, Drenkow J, Zaleski C, Jha S, et al.: STAR: ultrafast universal RNA-seq aligner. *Bioinformatics (Oxford, England),* 29**:** 15-21, 2013 10.1093/bioinformatics/bts635

51. Li B, Dewey CN: RSEM: accurate transcript quantification from RNA-Seq data with or without a reference genome. *BMC bioinformatics,* 12**:** 323, 2011 10.1186/1471-2105-12-323

52. Deshpande V, Park E, Jayatissa NU, Khan S, Mejia R, Yang CR, et al.: Bayesian mapping of protein kinases to vasopressin-regulated phosphorylation sites in renal collecting duct. *American journal of physiology Renal physiology,* 327**:** F591-F598, 2024 10.1152/ajprenal.00142.2024

53. Hino S, Tanji C, Nakayama KI, Kikuchi A: Phosphorylation of beta-catenin by cyclic AMP-dependent protein kinase stabilizes beta-catenin through inhibition of its ubiquitination. *Mol Cell Biol,* 25**:** 9063-9072, 2005 10.1128/MCB.25.20.9063-9072.2005

54. Leo KT, Chou CL, Yang CR, Park E, Raghuram V, Knepper MA: Bayesian analysis of dynamic phosphoproteomic data identifies protein kinases mediating GPCR responses. *Cell Commun Signal,* 20**:** 80, 2022 10.1186/s12964-022-00892-6

55. Haegel H, Larue L, Ohsugi M, Fedorov L, Herrenknecht K, Kemler R: Lack of beta-catenin affects mouse development at gastrulation. *Development,* 121**:** 3529-3537, 1995 10.1242/dev.121.11.3529

56. Knepper MA, Danielson RA, Saidel GM, Post RS: Quantitative analysis of renal medullary anatomy in rats and rabbits. *Kidney international,* 12**:** 313-323, 1977 10.1038/ki.1977.118

57. Hardcastle TJ: Generalized empirical Bayesian methods for discovery of differential data in high-throughput biology. *Bioinformatics (Oxford, England),* 32**:** 195-202, 2016 10.1093/bioinformatics/btv569

58. Korver W, Roose J, Clevers H: The winged-helix transcription factor Trident is expressed in cycling cells. *Nucleic Acids Res,* 25**:** 1715-1719, 1997 10.1093/nar/25.9.1715

59. Wang X, Kiyokawa H, Dennewitz MB, Costa RH: The Forkhead Box m1b transcription factor is essential for hepatocyte DNA replication and mitosis during mouse liver regeneration. *Proceedings of the National Academy of Sciences of the United States of America,* 99**:** 16881-16886, 2002 10.1073/pnas.252570299

60. Wang IC, Chen YJ, Hughes D, Petrovic V, Major ML, Park HJ, et al.: Forkhead box M1 regulates the transcriptional network of genes essential for mitotic progression and genes encoding the SCF (Skp2-Cks1) ubiquitin ligase. *Mol Cell Biol,* 25**:** 10875-10894, 2005 10.1128/MCB.25.24.10875-10894.2005

61. Polyak K, Lee MH, Erdjument-Bromage H, Koff A, Roberts JM, Tempst P, et al.: Cloning of p27Kip1, a cyclin-dependent kinase inhibitor and a potential mediator of extracellular antimitogenic signals. *Cell,* 78**:** 59-66, 1994 10.1016/0092-8674(94)90572-x

62. Matsuoka S, Edwards MC, Bai C, Parker S, Zhang P, Baldini A, et al.: p57KIP2, a structurally distinct member of the p21CIP1 Cdk inhibitor family, is a candidate tumor suppressor gene. *Genes Dev,* 9**:** 650-662, 1995 10.1101/gad.9.6.650

63. Yu J, Carroll TJ, Rajagopal J, Kobayashi A, Ren Q, McMahon AP: A Wnt7b-dependent pathway regulates the orientation of epithelial cell division and establishes the cortico-medullary axis of the mammalian kidney. *Development,* 136**:** 161-171, 2009 10.1242/dev.022087

64. Gunaratne R, Braucht DW, Rinschen MM, Chou CL, Hoffert JD, Pisitkun T, et al.: Quantitative phosphoproteomic analysis reveals cAMP/vasopressin-dependent signaling pathways in native renal thick ascending limb cells. *Proceedings of the National Academy of Sciences of the United States of America,* 107**:** 15653-15658, 2010 10.1073/pnas.1007424107

65. Nourse J, Firpo E, Flanagan WM, Coats S, Polyak K, Lee MH, et al.: Interleukin-2-mediated elimination of the p27Kip1 cyclin-dependent kinase inhibitor prevented by rapamycin. *Nature,* 372**:** 570-573, 1994 10.1038/372570a0

66. Sherr CJ, Roberts JM: Inhibitors of mammalian G1 cyclin-dependent kinases. *Genes Dev,* 9**:** 1149-1163, 1995 10.1101/gad.9.10.1149

67. Yan Y, Frisen J, Lee MH, Massague J, Barbacid M: Ablation of the CDK inhibitor p57Kip2 results in increased apoptosis and delayed differentiation during mouse development. *Genes Dev,* 11**:** 973-983, 1997 10.1101/gad.11.8.973

68. Zhang P, Liegeois NJ, Wong C, Finegold M, Hou H, Thompson JC, et al.: Altered cell differentiation and proliferation in mice lacking p57KIP2 indicates a role in Beckwith-Wiedemann syndrome. *Nature,* 387**:** 151-158, 1997 10.1038/387151a0

69. Westbury J, Watkins M, Ferguson-Smith AC, Smith J: Dynamic temporal and spatial regulation of the cdk inhibitor p57(kip2) during embryo morphogenesis. *Mech Dev,* 109**:** 83-89, 2001 10.1016/s0925-4773(01)00512-3

70. Takemaru KI, Moon RT: The transcriptional coactivator CBP interacts with beta-catenin to activate gene expression. *The Journal of cell biology,* 149**:** 249-254, 2000 10.1083/jcb.149.2.249

Table 1. *Gene Ontology Biological Process* terms over-represented in microdissected CCDs of Ser552Ala mutant vs. wild-type mice based on (A) upregulated transcripts and (B) downregulated transcripts.

A. Upregulated Transcripts

Term	% of Total	*P* (Fisher Exact)	Fold Enrichment	Transcripts
mitotic cell cycle process	37.5	8.2×10^{-11}	7.91	Plk1,Cdca8,Kif22,Cdc6,Foxm1,Aurkb, Ncaph,Anln,Prc1,Stmn1,Cdk1,Mcm3,Birc5, Ect2,Dlgap5
mitotic cytokinesis	17.5	8.8×10^{-10}	34.63	Anln,Plk1,Stmn1,Cdca8,Birc5,Ect2,Aurkb
nuclear division	27.5	9.3×10^{-9}	9.40	Top2A,Prc1,Plk1,Stmn1,Cdca8,Birc5,Kif22, Cdc6,Dlgap5,Ncaph,Aurkb
spindle organization	17.5	6.3×10^{-7}	13.52	Prc1,Plk1,Stmn1,Cdca8,Birc5,Dlgap5, Aurkb
G2/M transition of mitotic cell cycle	15	8.3×10^{-7}	17.97	Plk1,Cdk1,Birc5,Cdc6,Foxm1,Aurkb
regulation of cell cycle process	22.5	2.3×10^{-5}	5.48	Prc1,Plk1,Cdk1,Cdca8,Birc5,Cdc6,Ect2, Ncaph,Aurkb
microtubule cyto-skeleton organization	17.5	5.8×10^{-4}	4.67	Prc1,Plk1,Stmn1,Cdca8,Birc5,Dlgap5, Aurkb
DNA metabolic process	20	3.6×10^{-3}	3.04	Top2a,Cdk1,Mcm3,Cyp1b1,Kif22,Cdc6, Foxm1,Aurkb
apoptotic process	25	7.2×10^{-3}	2.34	Top2a,Plk1,Ifi203,Cdk1,Cyp1b1,Birc5, S100a14,Ect2,Tlr4,Aurkb

B. Downregulated Transcripts

Term	% of Total	*P* (Fisher Exact)	Fold Enrichment	Transcripts
animal organ development	28.33	6.5×10^{-3}	1.81	Cdkn1c,Egln1,Ctla2a,Brd1,Cdkn1b,Nfix,Cebpd, Tshz1,Cul3,Csnk2a2,Ush1c,2810429I04RIK, Ajap1,Oc90,H4c18,Gcnt2,Zfpm1

* Calculations carried out using *Database for Annotation, Visualization and Integrated Discovery* (DAVID) at https://david.ncifcrf.gov/. Background gene list included all transcripts with mean TPM>1.

Table 2. Transcripts corresponding to collecting duct principal cell marker genes: RNA-seq in microdissected CCDs from wild-type and Ser552Ala mutant mice

Gene Symbol	Annotation	Wild-type mean TPM	Mutant mean TPM	log_2 (Mutant/ Wildtype)	*P*
Acer2	alkaline ceramidase 2	50.2	52.7	0.07	0.597
Aqp2	aquaporin 2	17256.9	15649.1	-0.14	0.497
Aqp3	aquaporin 3	4388.3	4502.5	0.04	0.721
Aqp4	aquaporin 4	173.2	198.0	0.19	0.688
Atp1a1	ATPase, Na+/K+ transporting, alpha 1 polypeptide	450.7	397.6	-0.18	0.264
Atp1b1	ATPase, Na+/K+ transporting, beta 1 polypeptide	1179.5	1230.9	0.06	0.102
Avpr2	arginine vasopressin receptor 2	1032.7	1055.2	0.03	0.836
Clcnkb	chloride channel, voltage-sensitive Kb	1619.7	1615.2	0.00	0.959
Fxyd2	FXYD domain-containing ion transport regulator 2	981.6	747.8	-0.39	0.168
Fxyd4	FXYD domain-containing ion transport regulator 4	5855.2	6513.7	0.15	0.413
Fzd1	frizzled class receptor 1	45.2	47.0	0.06	0.675
Gata3	GATA binding protein 3	126.6	122.6	-0.05	0.575
Kcnj1	potassium inwardly-rectifying channel, subfamily J, member 1	987.6	1050.6	0.09	0.464
Lgals3	lectin, galactose binding, soluble 3	1616.4	1667.3	0.04	0.419
Lpar1	lysophosphatidic acid receptor 1	9.3	11.0	0.24	0.110
Npy6r	neuropeptide Y receptor Y6	31.4	34.3	0.13	0.516
Nr3c2	mineralocorticoid receptor	85.5	77.9	-0.13	0.044
Ptger4	prostaglandin E receptor 4 (subtype EP4)	21.3	20.8	-0.03	0.832
Ptges	prostaglandin E synthase	260.2	242.9	-0.10	0.380
Scnn1a	sodium channel, nonvoltage-gated 1 alpha	396.8	434.3	0.13	0.066
Scnn1b	sodium channel, nonvoltage-gated 1 beta	1079.6	1113.0	0.04	0.368
Scnn1g	sodium channel, nonvoltage-gated 1 gamma	777.9	809.3	0.06	0.247
Stc1	stanniocalcin 1	57.2	63.5	0.15	0.377
Tmem45b	transmembrane protein 45b	668.0	666.6	0.00	0.968
Tspan1	tetraspanin 1	633.1	633.7	0.00	0.993

* Collecting duct principal cell marker genes from https://esbl.nhlbi.nih.gov/Signaling-Pathways/PC-Diff-Markers/

Abbreviations: TPM, transcripts per million; *P*, *P* value from t-statistic.

Figure Legends

Figure 1. Primary structure of β-catenin showing phosphorylation sites and key domains. The total length in mouse is 781 amino acids (UniProt Accession: Q02248). Original image drawn *with NHLBI-AbDesigner* software (https://esbl.nhlbi.nih.gov/AbDesigner/).[25] Hydrophilicity calculated using the Kyte-Doolittle algorithm.[26] Ser552, phosphorylated in response to vasopressin in collecting duct principal cells, lies amid Armadillo Repeat Domain 10, which overlaps the site of binding of histone acetyltransferases CREB-binding protein (CBP) and p300. These histone acetyltransferases regulate chromatin accessibility by increasing histone acetylation, especially at histone H3 lysine-27 (H3K27Ac). Canonical regulation in the *Wnt* pathway is achieved through phosphorylation of a series of serines near the N-terminus of β-catenin by the protein kinases, casein kinase 1 (CK1) and glycogen-synthase kinase 3 β (GSK3β). Vinculin (Vcl) binding to the N-terminus facilitates β-catenin binding to cell-cell junctions. COOH-terminus interacts with the PDZ protein tax-interacting protein (TIP-1) to inhibit transcription of β -catenin target genes.[27]

Figure 2. Phosphorylation of β-catenin at Ser552 is dependent on protein kinase A (PKA) in mouse mpkCCD cells. A. Immunoblotting showing changes in β-catenin phosphorylation in response to vasopressin analog desmopressin (dDAVP) for different exposure times. B. Band density analysis for all replicates. C. Immunoblotting showing effect of deletion of both PKA catalytic genes on β-catenin phosphorylation. "PKA Substrates" shows phosphorylation detected with an antibody targeted to detection of all PKA-target sites. D. Band density analysis for all replicates. ** indicates $P < 0.01$. NS, not significantly different. Antibodies: anti-CTNNB1 antibody (rabbit, 1:1000, Cell signaling # 9562), anti-phospho CTNNB1 (Ser675) antibody (rabbit, 1:1000, Cell signaling # 9567), anti-phospho CTNNB1 (Ser552) antibody (rabbit, 1:1000, Cell signaling # 9566), anti-phospho PKA substrates (RRXS/T) antibody

(rabbit, 1:1000, Cell signaling # 9624) or anti-aquaporin-2 (rabbit, 1:1000, Knepper Lab, #K5007). Secondary antibody is goat anti-rabbit IRDye 680 (LI-COR).

Figure 3. The effects of Ser552Ala mutation versus wild-type (WT) mice on β-catenin phosphorylation, urine osmolality, and epithelial polarity. A. Sanger sequencing demonstrates successful sequence modification in nuclei of Ser552Ala mutant versus WT mice. B. Immunoblotting of whole inner medullas with the phospho-Ser552 antibody shows reduced phosphorylation in heterozygote (Het) and no phosphorylation in homozygote (Ho) with no loss of total β-catenin. C. Immunoblotting of nuclear fractions from inner medullas show no changes in total β-catenin in nuclei of Ser552Ala mutant versus WT mice. D. Densitometry of immunoblots shows no change in nuclear abundance of total β-catenin in Ser552Ala mutant mice versus WT mice. NS, not significant. E. Urine osmolality in daytime untimed ("spot") urine collections in Ser552Ala mutant versus WT mice. F. Lack of effect of Ser552Ala mutation on polarity of microdissected cortical collecting ducts as indicated by labeling of ZO-1 (a tight junction marker) and Na^+-K^+-ATPase (ATP1A1, a basolateral membrane marker). Scale bar, 10 µm. Antibodies: anti-ZO-1 (mouse, Invitrogen # 33-9100) and anti-Na^+/K^+ ATPase (rabbit, Knepper Lab, #H7642)[45]. The other antibodies are described in the legend to Figure 2.

Figure 4. Cortical branching and tubule size in Ser552Ala mutant mice versus wild-type (WT) mice. A. A highly branched cortical structure microdissected from mouse renal cortex showing that several DCTs converge into a single CCD. Scale bar, 100 µm. Antibodies: anti-Na^+/K^+ ATPase (ATP1A1, Millipore, #05-369-25UG), anti-thiazide-sensitive Na-Cl cotransporter (SLC12A3, Knepper Lab, #4375), and anti-parvalbumin (PVALB, Swant, #GP72). B. Diagram of idealized cortical branching structure demonstrating the approach to quantification of nephron:CCD branching ratio based on counting MTALs (green) and OMCDs (red) in cross sections of mouse inner stripe of outer medulla. C and D. Examples of cross sections of inter stripe of outer medulla labeled for the bumetanide-sensitive Na^+-K^+-$2Cl^-$ cotransporter (green) and aquaporin-2 (red) in WT and Ser552Ala mutant mice, respectively. Scale bar,

50 µm. Antibodies: anti-aquaporin-2 (rabbit, 1:500, Knepper Lab, #K5007) or anti-NKCC2 (chicken, 1:500, Knepper Lab #5198). E. MTAL:OMCD ratio quantification (cortical branching index) in WT versus Ser552Ala mutant mice. ***, $P < 0.001$. F. MTAL count per unit cross sectional area in WT versus Ser552Ala mutant mice. NS, not significantly different. G. OMCD count per unit cross sectional area in WT versus Ser552Ala mutant mice. *, $P < 0.05$. H. Quantification of OMCD diameter and cross-sectional area in WT versus Ser552Ala mutant mice. **, $P < 0.01$; *, $P < 0.05$. I. Quantification of MTAL diameter and cross-sectional area in WT versus Ser552Ala mutant mice. NS, not significantly different.

Figure 5. Immunofluorescence-labeled ducts of Bellini in the renal papilla from wild-type (WT) versus Ser552Ala mutant mice. A mouse kidney inner medulla was excised, and the renal papilla was dissected out. The renal papilla was fixed in 4% paraformaldehyde, further processed with alcohol and xylene, and embedded in paraffin blocks. Mouse renal papillae were prepared for either longitudinal or cross-sections and then labeled by immunofluorescence staining. A. Longitudinal section of the renal papilla showed the ducts of Bellini, labeled for aquaporin-2 (red) and anti-Na^+/K^+ ATPase (green). Scale bar, 100 µm. B. Cross-section of the renal papilla showing the ducts of Bellini at the end of the renal papilla (upper panel: within 25 µm from the end) and their increased numbers at higher levels (lower panel: 75 µm from the end). Tissue labeled for aquaporin-2 (red) and anti-Na^+/K^+ ATPase (green). Scale bar, 100 µm. Antibodies: anti-aquaporin-2 (rabbit, 1:500, Knepper Lab, #K5007), anti-Na^+/K^+ ATPase (mouse, 1:400, Millipore, #05-369-25UG). C. The total numbers of IMCDs at different distances from the end of the renal papilla (25 µm, 75 µm, or 125 µm) in WT (blue) versus Ser552Ala mutant mice (pink).

Figure 6. Volcano plot representation of transcriptomic changes in microdissected mouse cortical collecting ducts (CCDs) from Ser552Ala mutant versus wild-type (WT) mice. TPM, transcripts per million. *P* is derived from the t-statistic in a comparison of four Ser552Ala mutant mice versus four WT mice. Three technical replicates (separate microdissected CCDs) were used to calculate a mean value for each animal. Gene symbols on the right indicate increased transcripts that match the *Gene Ontology*

Biological Process term “mitotic cell cycle process”. Downregulated transcripts on the left indicated decreased transcripts that map to the *Gene Ontology Biological Process* term “animal organ development”.

Figure 7. Nuclear counting and cell cycle indices in immunofluorescence-labeled microdissected cortical collecting ducts (CCDs) from Ser552Ala mutant versus wild-type (WT) mice. After microdissection, CCDs were fixed with 4% paraformaldehyde, followed by labeling for aquaporin-2 and for nuclei using 4',6-diamidino-2-phenylindole (DAPI). A. IMARIS-generated confocal immunofluorescent analytical image of microdissected CCDs from WT and Ser552Ala mutant mice. Aquaporin-2 is labeled in red. Nuclei are labeled with DAPI and shown in grayish purple based on IMARIS “spot” analysis tools. Scale bar, 10 µm. Antibodies: anti-aquaporin-2 (rabbit, 1:500, Knepper Lab, #K5007). B and C. Nuclei per length and tubular diameter of microdissected CCDs in WT versus Ser552Ala mutant mice. *, $P < 0.05$; NS, not significantly different. D. Histogram of DAPI immunofluorescence intensity in nuclei from microdissected CCDs of WT and Ser552Ala mutant mice. The x-axis represents DAPI-labeled single-nucleus intensity, and the y-axis represents the number of nuclei. The blue and pink bars indicate the number of nuclei for WT and mutant mice, respectively with overlaid density curves for each group. A green dashed line marks the threshold for “high-intensity” nuclei (defined as the mean plus one standard deviation of total immunofluorescence).

Figure 8. Schematic diagram summarizing structural parameters in wild-type (WT) and Ser552Ala mutant mice. The diagram provides a visual representation of tubule branching patterns, highlighting the structural organization and differences in branching ratios in WT and Ser552Ala mutant mice. Glomerular counts show approximately equal nephron numbers (n = 13,600 in WT mice, n = 13,500 in Ser552Ala mutant mice). Distal convoluted tubules (DCTs) connect to connecting tubules (CNT) which undergo convergence through branched CNTs and initial collecting tubules (iCTs) and then connect to a cortical collecting duct (CCD). The medullary thick ascending limb (MTAL)/outer medullary collecting

duct (OMCD) ratio, which quantifies the numbers of nephrons converging into an unbranched collecting duct, averaged 6.2 in WT mice and 3.3 in Ser552Ala mutant mice. The unbranched collecting ducts (CCD/OMCD) are more numerous in the mutant mice (n = 2,200 in WT mice, n = 4,100 in Ser552Ala mutant mice. The convergence of collecting ducts resumes in the inner medulla, eventually reducing IMCD number (ducts of Bellini) to 6.33 in WT mice and 6.67 in Ser552Ala mutant mice.

(Figure 1)

Diagram of β-Catenin Showing Phosphorylation Sites and Key Domains

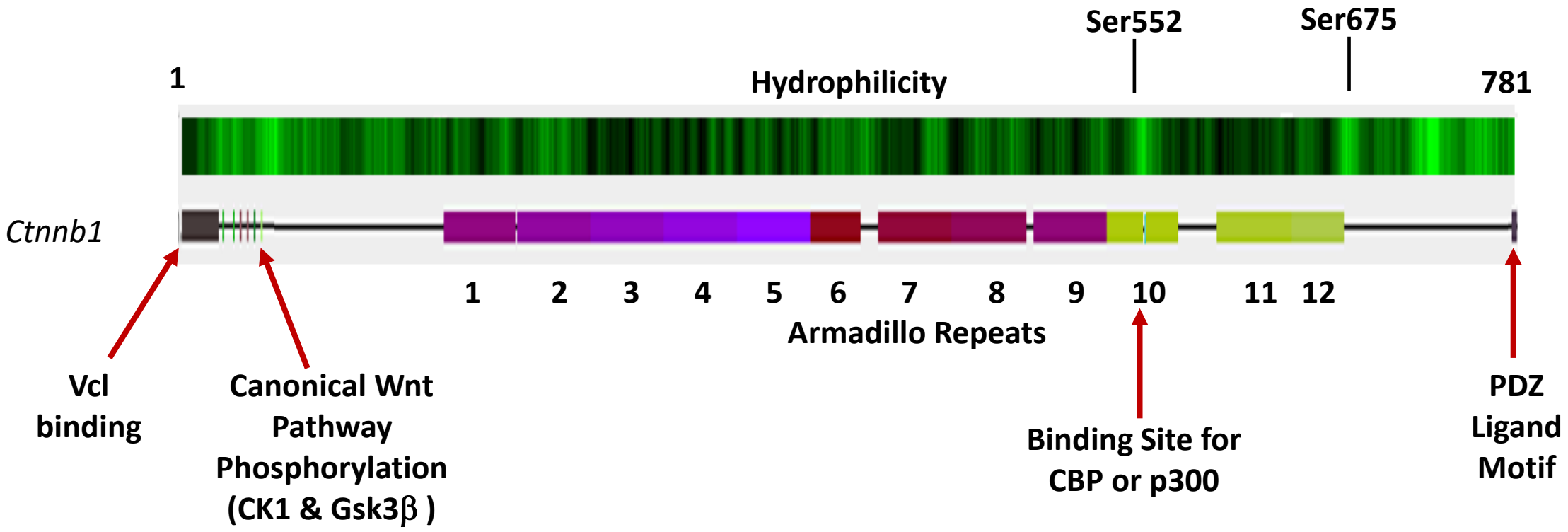

(Original image drawn *with NHLBI-AbDesigner* software)

(Figure 2)

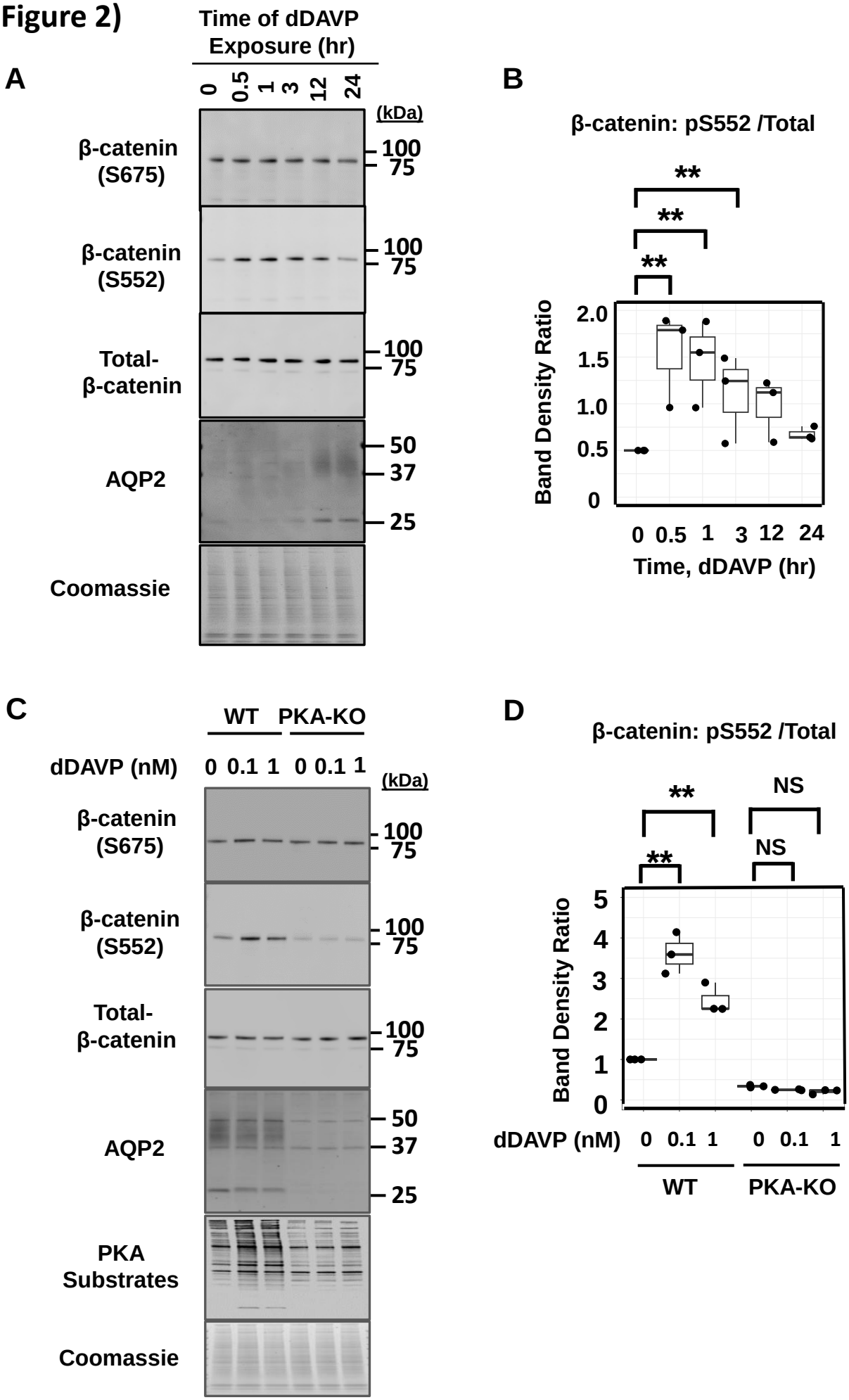
A
Time of dDAVP Exposure (hr)
0
0.5
1
3
12
24
(kDa)
β-catenin (S675)
β-catenin (S552)
Total-β-catenin
AQP2
Coomassie
100
75
50
37
25
B
β-catenin: pS552 /Total
**
**
**
Band Density Ratio
2.0
1.5
1.0
0.5
0
0 0.5 1 3 12 24
Time, dDAVP (hr)
C
WT
PKA-KO
dDAVP (nM)
0 0.1 1 0 0.1 1
(kDa)
β-catenin (S675)
β-catenin (S552)
Total-β-catenin
AQP2
PKA Substrates
Coomassie
100
75
50
37
25
D
β-catenin: pS552 /Total
**
NS
**
NS
Band Density Ratio
5
4
3
2
1
0
dDAVP (nM)
0 0.1 1 0 0.1 1
WT
PKA-KO

(Figure 3)

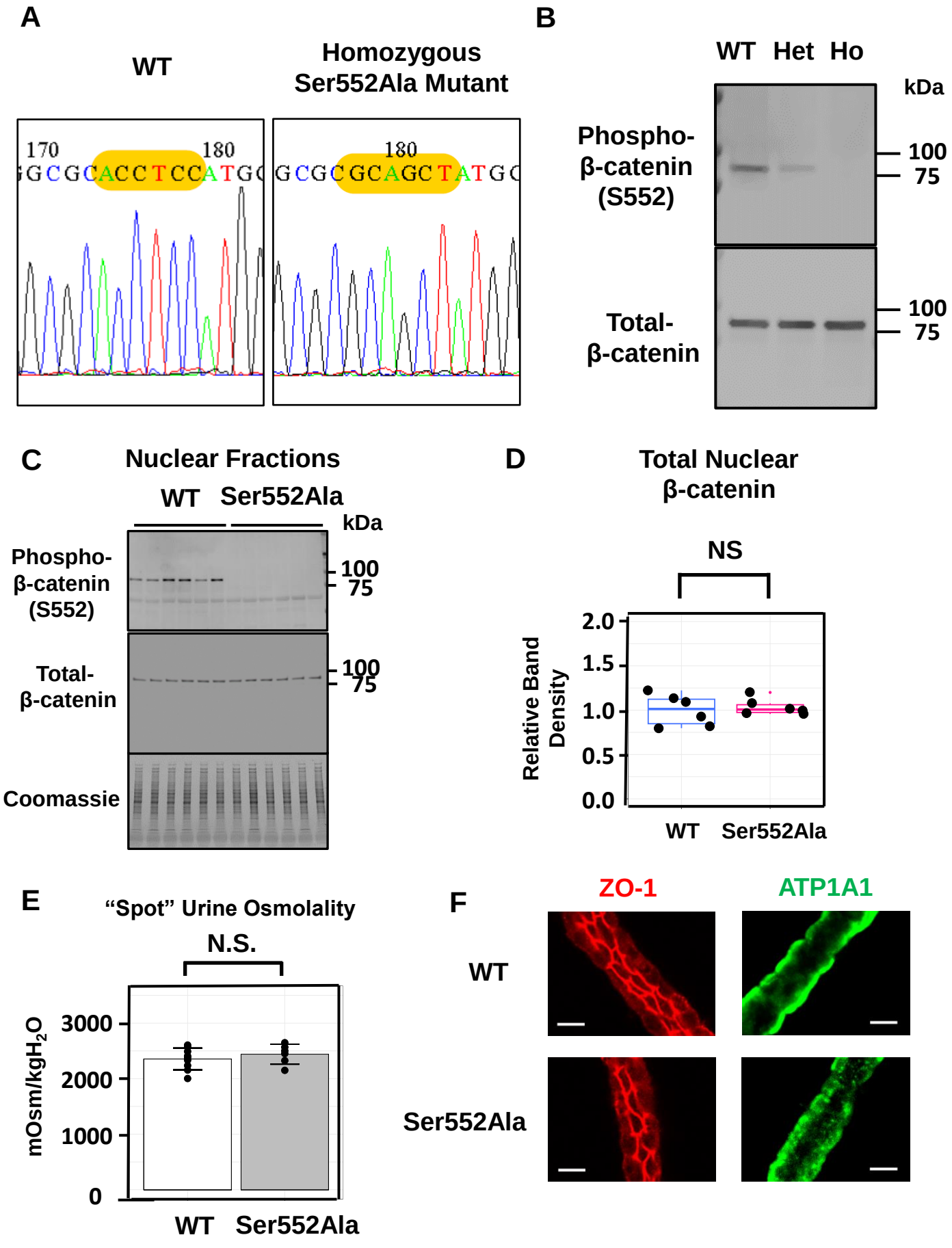
A
WT
Homozygous
Ser552Ala Mutant
170
180
GGCGCACCTCCATGC
180
GCGCGCAGCTATGC
B
WT Het Ho
kDa
Phospho-
β-catenin
(S552)
100
75
Total-
β-catenin
100
75
C
Nuclear Fractions
WT Ser552Ala
kDa
Phospho-
β-catenin
(S552)
100
75
Total-
β-catenin
100
75
Coomassie
D
Total Nuclear
β-catenin
NS
Relative Band
Density
2.0
1.5
1.0
0.5
0.0
WT Ser552Ala
E
"Spot" Urine Osmolality
N.S.
mOsm/kgH2O
3000
2000
1000
0
WT Ser552Ala
F
ZO-1
ATP1A1
WT
Ser552Ala

(Figure 4)

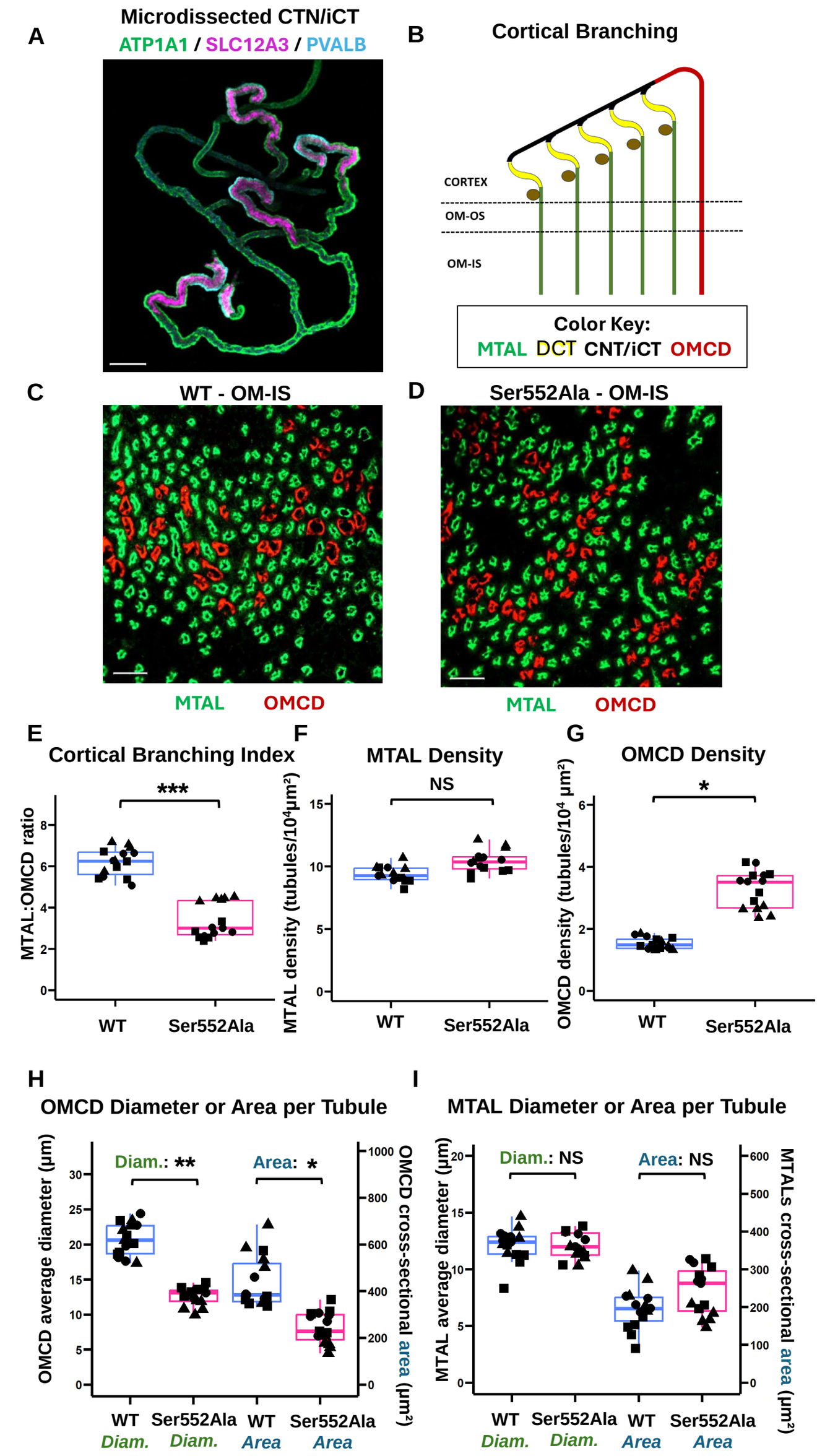
A
Microdissected CTN/iCT
ATP1A1 / SLC12A3 / PVALB
B
Cortical Branching
CORTEX
OM-OS
OM-IS
Color Key:
MTAL DCT CNT/iCT OMCD
C
WT - OM-IS
MTAL OMCD
D
Ser552Ala - OM-IS
MTAL OMCD
E
Cortical Branching Index
***
MTAL:OMCD ratio
WT
Ser552Ala
F
MTAL Density
NS
MTAL density (tubules/10⁴µm²)
WT
Ser552Ala
G
OMCD Density
*
OMCD density (tubules/10⁴ µm²)
WT
Ser552Ala
H
OMCD Diameter or Area per Tubule
Diam.: **
Area: *
OMCD average diameter (µm)
OMCD cross-sectional area (µm²)
WT Diam.
Ser552Ala Diam.
WT Area
Ser552Ala Area
I
MTAL Diameter or Area per Tubule
Diam.: NS
Area: NS
MTAL average diameter (µm)
MTALs cross-sectional area (µm²)
WT Diam.
Ser552Ala Diam.
WT Area
Ser552Ala Area

(Figure 5)

A

Longitudinal section

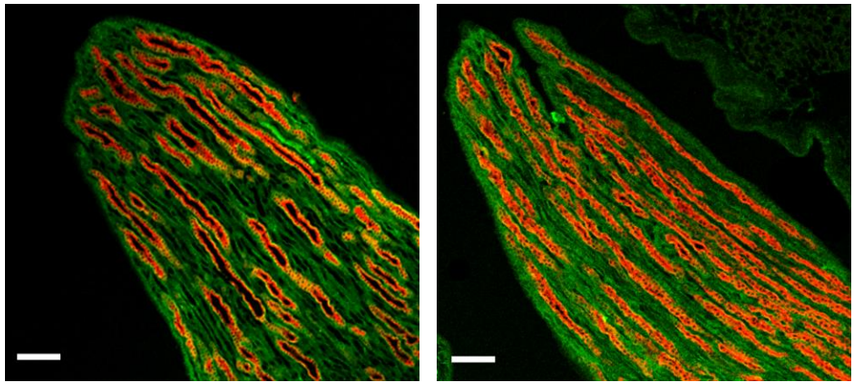

AQP2/ATP1A1

B

Cross section

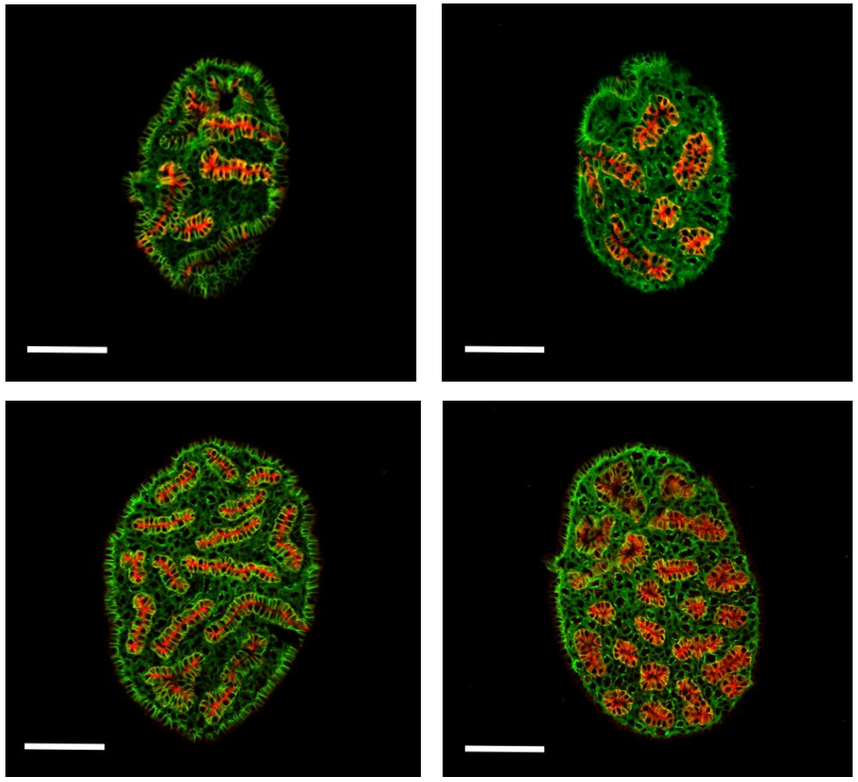

AQP2/ATP1A1

C

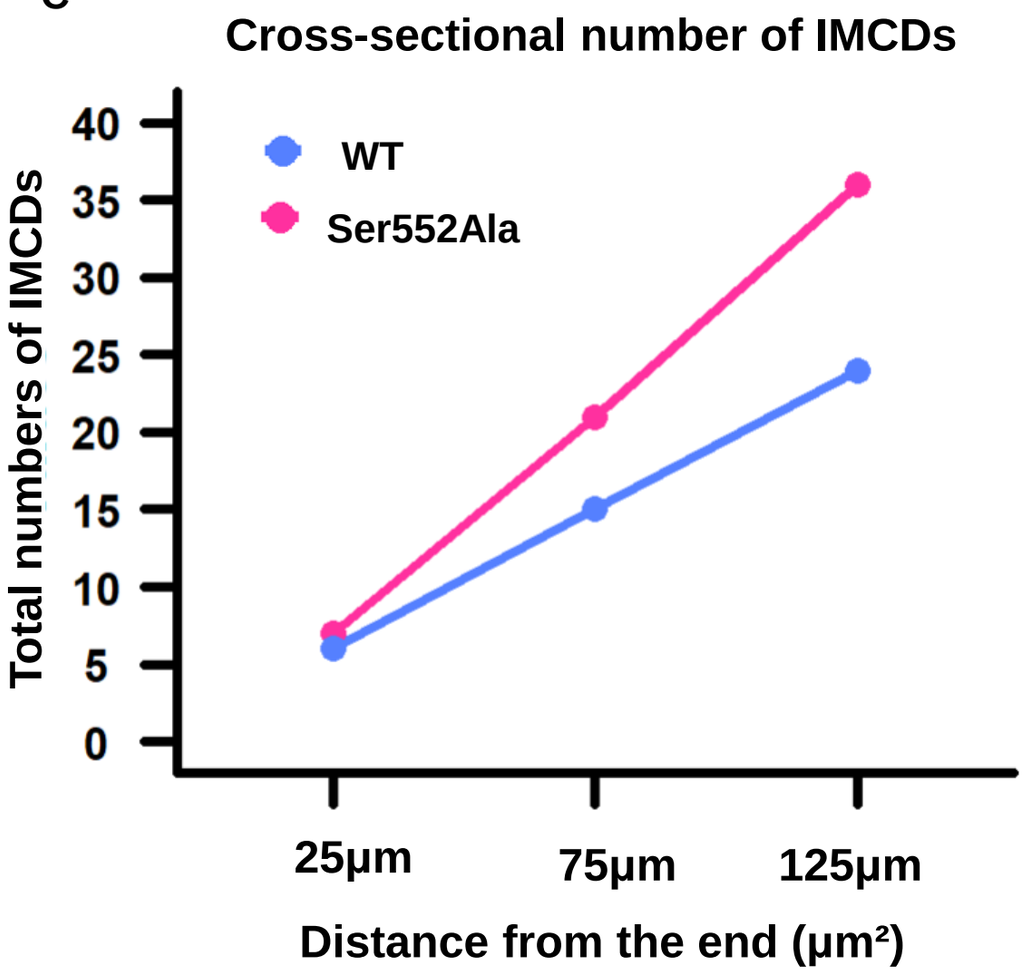

(Figure 6) RNA-Seq in Microdissected Cortical Collecting Ducts

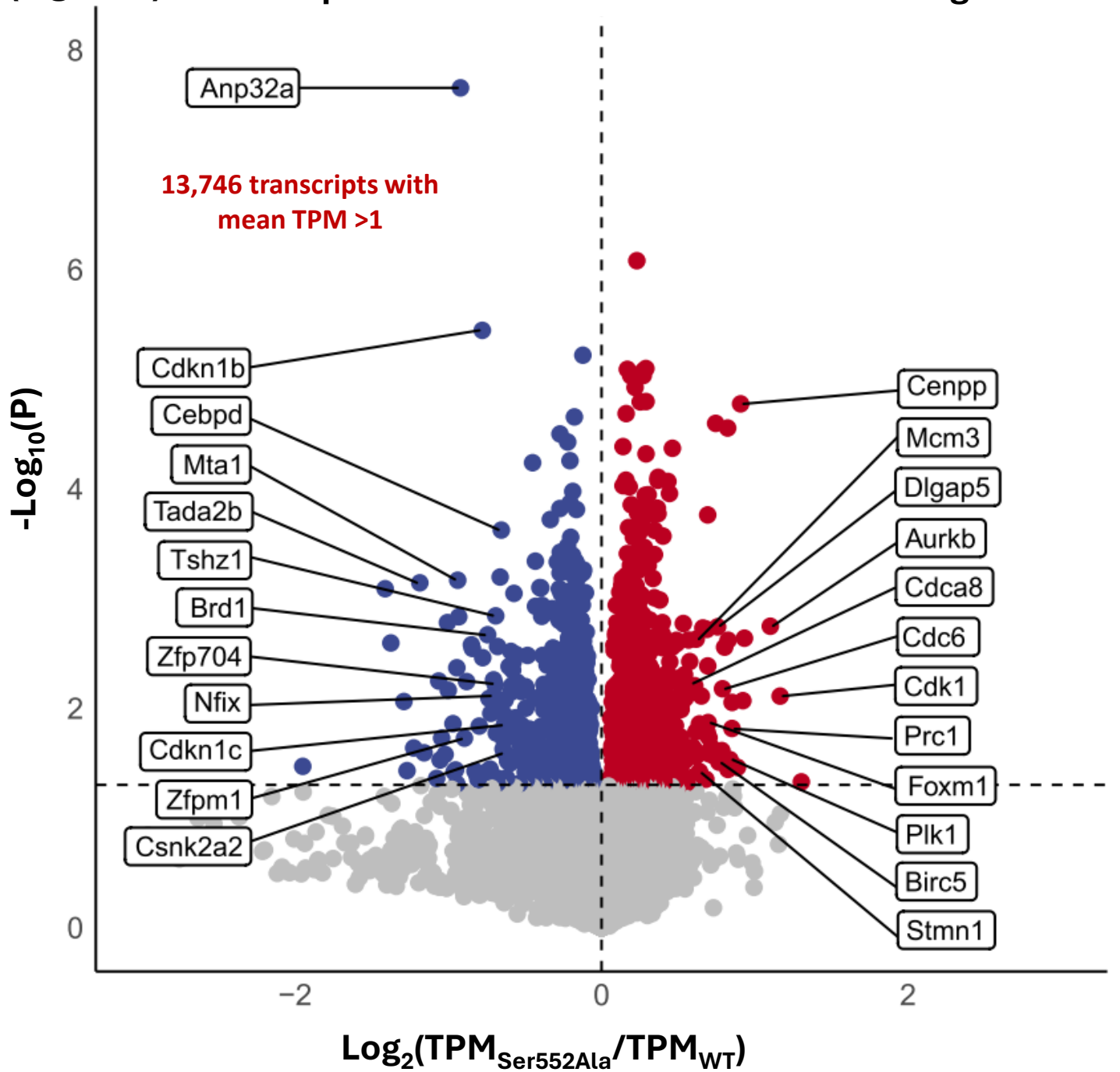

(Figure 7)

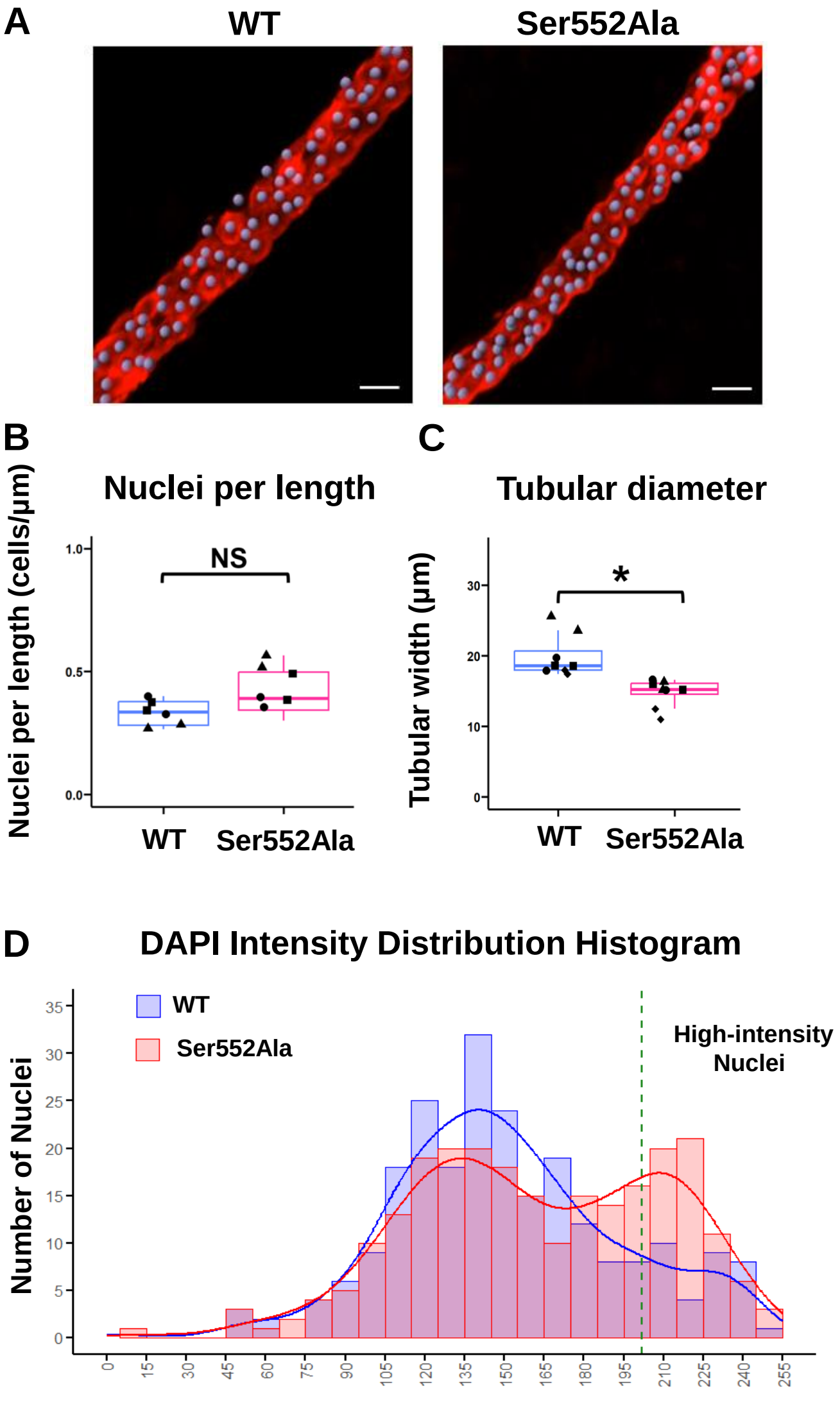
A
WT
Ser552Ala
B
Nuclei per length
Nuclei per length (cells/µm)
NS
1.0
0.5
0.0
WT
Ser552Ala
C
Tubular diameter
Tubular width (µm)
*
30
20
10
0
WT
Ser552Ala
D
DAPI Intensity Distribution Histogram
Number of Nuclei
WT
Ser552Ala
High-intensity Nuclei
35
30
25
20
15
10
5
0
0
15
30
45
60
75
90
105
120
135
150
165
180
195
210
225
240
255

(Figure 8)

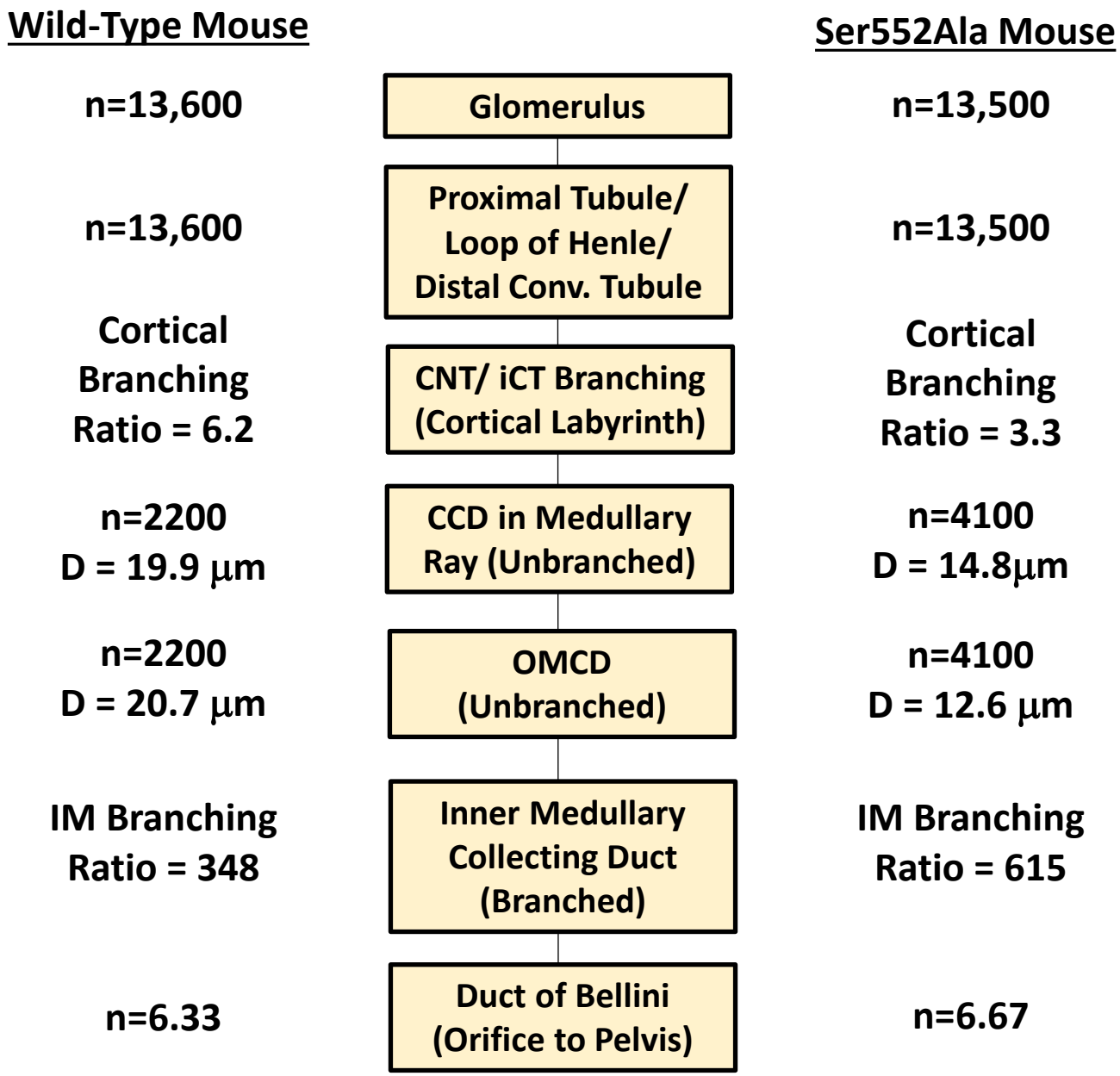
Wild-Type Mouse
Ser552Ala Mouse
n=13,600
Glomerulus
n=13,500
n=13,600
Proximal Tubule/ Loop of Henle/ Distal Conv. Tubule
n=13,500
Cortical Branching Ratio = 6.2
CNT/ iCT Branching (Cortical Labyrinth)
Cortical Branching Ratio = 3.3
n=2200
D = 19.9 μm
CCD in Medullary Ray (Unbranched)
n=4100
D = 14.8μm
n=2200
D = 20.7 μm
OMCD (Unbranched)
n=4100
D = 12.6 μm
IM Branching Ratio = 348
Inner Medullary Collecting Duct (Branched)
IM Branching Ratio = 615
n=6.33
Duct of Bellini (Orifice to Pelvis)
n=6.67